International Journal of Machine Tools and Manufacture, Volume 49, Issues 12-13, October 2009, Pages 998-1007

Ultra-precision grinding of PZT ceramics – Surface integrity control and tooling design contribution

S.ARAI[†] J.CORBETT R.W.WHATMORE and S.A.WILSON*

Materials Department, Cranfield University, Cranfield, Bedfordshire, MK43 0AL, United Kingdom

*Corresponding author: e-mail: s.a.wilson@cranfield.ac.uk Tel: +44 1234 750111 Fax: +44 1234 751346

[†] Current address: NSK Ltd. Manufacturing Engineering Center, Toriba - Machi 78, Maebashi – City, Gunma 371-8527, Japan

Abstract

A methodology for consistent surface integrity control in ultra-precision grinding of polycrystalline PZT ceramics is established through assessment of the interaction between the method of material removal and the machine design. In the first phase of experimentation, defects including porosity and fractural damage induced in the subsurface area were investigated. This was linked to a statistical analysis of cup wheel grinding conditions, which suggested previously unconsidered systematic models for the material removal process and which identified the optimum machining conditions required for excellent surface roughness and surface flatness with minimum textural damage. In verifying the suggested model, not only the grinding parameters but also control of the loop distance between the grinding wheel and the surface of the workpiece have been considered. Contact at the material removal interface was found to be of critical importance. This idea led to a design improvement for the tooling structure. It was concluded that viscoelastic damping and relatively soft contact at the material removal interface are beneficial in obtaining a fine surface finish together with a flat surface. This contrasts to previous work where researchers have claimed that high static loop stiffness and high resonant frequencies of machine structures are essential for this purpose.

Keywords

Fracture, thick film, micro-actuator, damping, soft contact, loop distance

1. Introduction

Polycrystalline lead zirconate titanate (PZT) ceramics are of major importance in microtechnology, particularly in the field of sensors and actuators, because of their superior piezoelectric and pyroelectric properties and their high dielectric constants (Setter, 2001; Uchino, 2004; Uchino, 2006; Wilson and Bowen, 2007). Devices that incorporate these materials as their active component include micro-pumps and valves, ultrasonic motors, thermal sensors, probes for medical imaging and non-destructive testing, accelerometers and quite recently a new range of electronic components that includes filters, memory devices and switches. The materials are well established and an extensive range of compositional variations are available that can be tailored to particular commercial devices. New applications continue to emerge, and a major research effort has been underway to address the manufacturing technology required to incorporate these materials with associated structural components and electronic circuitry at the wafer scale. In one such study, it has recently been demonstrated that micro-scale actuators can be assembled using ultra-precision grinding in association with standard micro-fabrication processes such as wafer bonding and photolithography (Wilson et al., 2006). Such devices are suitable for micro-fluidic or micro-pneumatic systems and the methods used lend themselves to batch production**.** Moreover the electromechanical properties of ultra-precision ground PZT layers in the 20 ~ 50 micron thickness range are far superior to those produced by alternative methods such as thick film deposition. Multi-layer thick PZT film devices and multi-material devices can potentially be fabricated by ultra-precision machining on an industrial scale, and this has been the motivation for the following investigation into fine surface integrity control.

In the field of precision machining, cutting and grinding processes are two of the most common techniques used to obtain appropriate geometry, even if the tolerance specification is at the sub-micron scale. A wide variety of materials can be processed in this way, including brittle materials, and a great deal of emphasis has been placed on the need to produce high surface quality. This is important, as micro-scale surface and sub-surface defects induced by machining can change the surface stress distribution, residual or applied, leading to a deterioration in mechanical performance and poor fatigue behavior. Much of the published work in this area is focused on the material-removal behavior of brittle materials at the microscopic scale. Similarly there is a body of work which discusses the design characterization of individual machine components, assuming that extremely high rigidity at the material removal area is ideal. However, a comprehensive evaluation of the significance of both of these factors together and their interdependence is difficult to find. This undoubtedly reflects the complexity of practical material removal, especially in precision grinding.

With regard to the machinability of piezoelectric ceramic materials, some studies exist which evaluate damage initiation in comparison to other brittle materials (Beltrao et al., 1997; Tanaka and Isono, 2001). Investigations have been carried out based on observations of crack propagation, leading to an evaluation of mechanical toughness in the sub-surface area. Importantly it has been shown in these studies that ductile material removal can be achieved with a very small depth of cut, close to the critical

depth of cut, which is defined as a boundary for damage-free surface finishing at the sub-micron scale. However, in polycrystalline PZT ceramics it is exceptionally difficult to perform ductile machining over an entire surface. This is chiefly because of the characteristic ferroelastic behaviour exhibited by these materials, (whereby the ferroelectric domain structure is reoriented by the application of an external force) which tends to cause some deterioration in the mechanical stress distribution of the workpiece as it is being machined (Beltrao, 1998) . The presence of weak grain boundaries, occasionally because of the presence of excess lead, in commercial PZT ceramic materials is a further contributing factor (Tanaka and Isono, 2001). Furthermore, it has been reported that the grinding direction has a significant influence on the variation of surface roughness and this was also associated with ferroelasticity (Beltrao et al., 1997).

A further critical factor in achieving an exceptionally fine quality of surface finish by precision cutting and grinding, is the mechanical performance of the machine tool components. This is directly associated with structural stability, and it influences the surface integrity control performance significantly. Precision machine tools have often been developed (with the objective of achieving the highest material removal rate and dimensional accuracy in the sub-micron range) by focusing on high structural stiffness. Mechanical characteristics such as thermal stability, static stability and dynamic stability are all regarded as being important factors required to achieve consistent accuracy of machine motion. In practice the totality of the system needs to be taken into account as structural variations, from vibration or drifting with time, can directly affect the loop distance between the tool and the workpiece. Hence they have a controlling influence on finished surface integrity (Inasaki, 2004).

2. Background

In grinding processes, relative displacement in the loop distance, which can be defined for machine tool structures as the distance between the tool and the workpiece, leads to a variation of the actual depth of cut. For ceramic materials this can cause brittle damage such as dislocations and localized cracking on the workpiece surface (Zhang et al., 2003). For polycrystalline PZT ceramics the quality of the ductile material removal mode is extremely sensitive to changes in the depth of cut from the critical value, which is observed to be ~ 200-400nm (Beltrao, 1998). Essentially this means that not only the design of the machine tool, but also the design characteristics of the grinding wheel, the tooling components and, furthermore, the contact manner at the material removal point should be controlled comprehensively, since these are all important in achieving such a fine depth of cut and consequently a ductile material removal mode. With this in mind, some requirements for ductile mode precision grinding of ceramics have been listed in outline below (Kanai et al., 1995).

- High contact stiffness or high abrasive support stiffness
- High abrasive protrusion
- No loose abrasives
- Controllability of random protrusion height distribution within 0.1 micrometer

For a more comprehensive treatment, several essential factors must be added to this simplified outline. In particular the performance of the grinding wheel should be discussed with respect to: a) the geometry and concentration of active abrasive grits; b) the kinematics of each abrasive grit engagement, which is determined by the setup parameters of the process (Warnecke and Barth 1999); c) the consistency of the machining environment including temperature variation at the grinding point and d) the fatigue behavior of the abrasive grits including bonding elements.

Meanwhile, the analysis of the material removal mechanism is not particularly easy in practical grinding even if the machine characteristics have been considered. This is mainly because microscopic material removal is continuously accomplished by multiple abrasive grits during grinding, and hence the finished surface only reflects their interactions. Because of this, simplified evaluations are commonly preferred. These have the advantage that the microscopic material removal behaviour of single fine abrasive grits can be observed clearly.

Static indentation or quasi-static (low speed) scratching tests, with various diamond single point indenters or knife edges are typically used for the material removal investigation of brittle workpieces (Malkin and Hwang, 1996; Inasaki, 1987; Marshall et al., 1983; Klocke and Hambucker, 1997). These methods enable the material removal mechanism to be isolated from other phenomena and only damage initiation processes on the surface are revealed. Hence it is possible to evaluate the transition factors between successful material removal in ductile mode and fractural damage initiation in brittle mode. For instance, fundamental crack propagation phenomena are usually realized with static indentation methods and the continuous material removal mechanism with moving indentation schemes. As a result, three different crack propagation modes have been identified and categorized, which are called median, lateral and radial cracks. It has also been understood from careful microscopic investigations that generation of plastically deformed areas and continuous stress release phenomena in the subsurface of a workpiece under the indented points are the major source of these cracks (Inasaki, 1987). When various PZT ceramics are inspected, however, these archetypal modes are not clearly observed and it has been claimed that this tendency is associated with the polycrystalline texture, existence of porosity and domain-switching effects (Fan et al., 1993). In practice, the heterogeneities and structural damage initiated in the surface and subsurface area of PZT ceramics, show features such as dislocations, voids, micro cracks, grain pull outs, interfacial failure of grains and redistribution of residual stresses. Since these can easily reduce the fracture toughness of the workpiece and shorten operational lifetime through reduced fatigue resistance, it can be stated that the mechanical performance characteristics of PZT ceramics are not easy to control (Corbett, 2001).

With respect to a general environmental control strategy in practical grinding, the influence of lubrication has been investigated by scratching tests for advanced ceramics (Desa and Bahadur, 1999). Studies showed that the highest material removal rates were achieved in dry conditions, and this was associated with maximal sub-surface damage. Lower removal rates were observed in water-lubricated conditions and this also resulted in reduced surface strength. Both effects seems to be explained

by formation of a hydrated oxide layer on the surface, leading to the notion that chemical reactions might also be significant factors when grinding ceramics. It has been suggested that mechano-chemical or electro-chemical reactions are key considerations for achieving mirror-quality or super-finished surfaces without secondary textural defects inside the workpiece materials (Editorial Office of Tool Engineers, 1990; Encyclopedia of New Machining Tools, 1991; Bifano et al., 1988).

Electro-active ceramics such as PZT exhibit some highly complex dynamic mechanical behaviour at the micro-scale. There is some variability associated with different material compositions, meaning that not all commercial grades are machinable in the same manner and typically there are also some physical inconsistencies such as porosity and dislocations (Beltrao, 1998). However, it can be generally summarized that PZT ceramics are significantly less hard and thus the stress concentrations in them are relatively low, when compared to other ceramics. On the other hand, it is also claimed that these materials are mechanically more sensitive to thermal transients than are other advanced ceramics. This is witnessed by changes in their pyroelectric and piezoelectric properties (Morgan Matroc Ltd, 2002). Furthermore, since domain switching in ferroelectric ceramics is characterized by rapid microscopic elastic deformations of each grain, there is a certain concomitant change in the stress regime within the textile structure that occurs during grinding (Tanaka and Isono, 2001).

As mentioned, residual stress in the subsurface area reflects structural capability and it also influences microscopic properties. Although the volumetric change within the surface or near-surface layer changes with each external loading condition (e.g. permanent volumetric compression of microstructures, plastic deformation of the surface layer due to thermal energy and plastic deformation of the surface layer due to impact force), it can be said that internal deformation of microstructures are the main reason for the development of residual stress (Griffiths, 2001). This implies that brittle damage such as subsurface cracking and/or grain pull out can also be a significant cause of variation in the residual stress distribution, because these fracture defects are initiated through plastic deformation and generation of dislocations during the machining process.

The ultra-precision machine tool used for the experimental part of this study was Tetraform C. This is an example of a precision machine tool that has been designed specifically to meet the requirement of extremely high stiffness for ultra-precision grinding of hard materials (Cranfield University and Loadpoint Ltd., UK). It has a tetrahedral frame consisting of several closed column loops, which contribute to high static and dynamic stability, enabling the machine to produce a ground surface quality on the nano-scale for a wide range of materials (Corbett et al., 2000; Corbett, 2001a; Corbett and Stephenson, 2001b; McKeown and Corbett, 2004, Corbett et al., 1999). A prototype machine Tetraform 1 was equipped with hydraulic damping devices inside the columns to ensure a high dynamic consistency (Slocum, 1992), however these were omitted for Tetraform C as it was found later that the tetrahedral structural frame itself had dominant damping properties. Tetraform C has a vertical grinding spindle axis and horizontal X and Y axis capability. Aerostatic bearings are used for the spindle unit, whereas the X-Y axes consisted of hydrostatic feed screws and guide

ways. Each linear axis is operated by a position control system, whose sensing and positioning resolutions are 10.0 nanometres and 1.0 micron respectively, controlled using a high resolution interferometric grating liner encoder (Heidenhain LIP 40R). Utilization of hydrostatic mechanical components is typical for this kind of machine tool to enhance the motion accuracy.

3. Investigation of Material Removal Behaviour

In the first phase of this research work, the microscopic damage propagation mechanism and the practical material removal mechanism of PZT ceramics were investigated in cup grinding mode using diamond abrasive grits. The fundamental machinability of the PZT ceramics was analyzed and the machined surfaces thoroughly examined. On the basis of these investigations a series of statistical grinding experiments was devised and an analysis of variance (ANOVA) was carried out in order to identify which significant technical factors can lead to enhancement of surface integrity. The results are discussed below with reference to the material removal behavior of PZT ceramics, not assuming a single point material removal model, but instead describing the interaction of multiple abrasive grits used in practical grinding.

3-1. Fundamental Evaluation of Damage Propagation

The initial surface damage investigations highlighted two key factors in the practical grinding of piezoelectric ceramics namely the relative weakness of the grain boundaries and a high sensitivity to heat generation.

Figure 1 shows two different microscopic optical views of the same area of a PZT ceramic surface, which was finished by polishing with fine alumina particles of 3.0 microns. By inspection of these surfaces, it was found that during the sintering process porosity was generated everywhere inside and between spherical textures, which range in size up to around 300 microns in diameter. This is an artifact of the mixed-oxide route used in manufacturing. Particles (sub-micron or a few microns in diameter) of the ceramic pre-cursor, which have been pretreated, crushed and mixed in order to enhance their reactivity, are bound together with a binding compound in a spray-and-dry process, producing many fine granules. The spherical texture (and the porosity) observed in Figure 1 is a result of the permanent binding phenomenon of the granules during high temperature sintering and it is understood that the generation of tiny pores is consistent with many commercial PZT ceramics.

It was realized from the micrographs that the porous discontinuities characteristically fall into two different modal types depending on their location. Hence the categories of ‘core’ and ‘boundary’ porosity are defined in this study as shown in Figure 1. Observations have subsequently confirmed that the pores do constitute potential sites for mechanical damage initiation, such as dislocation and micro-cracking. This is particularly true when a pore possesses an acute angled edge or several sharp edges at its boundary. These positions are extremely sensitive origins of stress concentration and consequently exhibit poor mechanical toughness. In a material removal process

with multipoint abrasive grits, these defects are subject to stress concentration both by the applied grinding force and its dynamic variation with time.

Figure 2 shows an extreme example of machining damage, resulting from this fractural phenomenon and leading to structural failure. Examination of the fracture-surface showed that the PZT ceramic disc has cracked along only one of the trace marks left by the grinding wheel. This occurred spontaneously some time after machining and it provides clear evidence that high stress concentration inside the bulk occurs due to the grinding force. Even if the mechanical damage is almost invisible after grinding and does not initially result in such a severe incident, there are obviously potential sources of failure where stress is concentrated and this also has consequences for the fatigue behaviour of the material.

With reference to the material properties of PZT ceramics, this fractural tendency can be explained by their high sensitivity to external forces and temperatures. Often this is attributed to the presence of dopants or excess lead, which tends to weaken the fracture toughness of the grain boundaries and causes high ductility at elevated temperatures (Tanaka and Isono, 2001). In this respect machinability can be viewed as only one of a suite of materials properties, along with the excellent pyroelectric and piezoelectric properties which also derive from the selective addition of dopants to the basic composition. Hence in practice some commercial grades of PZT show better machinability than others.

3-2. Modeling the Material Removal Behaviour

Since high concentration and continuous variation of the grinding forces were identified as major reasons for deterioration of the finished quality on PZT ceramic surfaces in the first phase of this research work, the next step sought to evaluate the relative importance of technical factors such as grinding parameters and material properties. Uniquely, the systematic engagement between the tool and the workpiece was also taken into account as a design factor (vertical compliance) for the tooling components. Although it is generally considered ideal to avoid unwanted movement between the grinding wheel and the workpiece surface during machining, it was considered this point should, even so, be scientifically evaluated for successful surface integrity control in ultra-precision grinding for these ceramics.

In order to compare the significance of such various technical factors comprehensively, the statistical analysis ANOVA was applied in the second phase of investigation. This methodology has the capability to highlight the technically significant factors which control the finished surface integrity with regard to the aspects of the microscopic material removal mode, machining environment, tooling design and also their respective interactions (Arai, 2004).

The interaction of the defined technical factors is very significant. It is both theoretically and practically known that appropriate combinations of spindle speed and feed rate can improve surface roughness in ultra-precision grinding, because these conditions can produce finer chip thickness, followed by ductile material removal (Stephenson et al., 2001) Furthermore, it also became evident from the initial grinding

trials that the workpiece tooling method has a strong influence on the consistency of the grinding forces. These tendencies imply that the interactions between each grinding parameter, including design contributions from the machine structure and tooling components, all influence stability at the material removal points and they also need to be taken into account when identifying the major influential factors for grinding PZT ceramics.

With this background, a statistical array of L_{16} (2^{15}), which possesses a high degree of freedom suitable for the significance analysis of many technical factors and their interactions, was designed for the grinding evaluation.

Table 1 shows the designed array for the series of statistical grinding experiments. The defined factors are A - feed rate, B - spindle speed, A×B, C - work piece material, A×C, B×C, A×B×C, D - abrasive grit size, A×D, F - work depth of cut, A×B×D, G - chuck design for work piece, A×G, C×F and A×B×G. There were two sets of statistical experiments, one performed with and one without ELID (electrolytic in-process dressing). This approach was used to consider the effect of the environmental control of grinding process. Resin and cast iron bonded cup grinding wheels with diamond abrasive grit sizes 3 ~ 6 and 6 ~ 12 microns, were used for each set of grinding experiments. Unpoled hard and soft PZT bulk ceramic workpieces (diameter 50 mm, thickness 2.0 mm), each having an average grain size of approximately 5 ~ 7 microns, were prepared for both experiments. The tooling devices used were a vacuum chuck, consisting simply of a bolted aluminum plate fixture, which provided little vertical compliance (high rigidity) and a porous ceramic fixture, which provided high vertical compliance (flexible elasticity) due to its flexible holding interface.

Table 2 (a) - (c) shows the results of the statistical evaluation for the grinding experiments without ELID. The general tendencies mainly reveal physical damage and the influence of heat generation, which are due to loading the elements on the grinding wheel. This is shown schematically in Figure 3 as workpiece chips which become stuck on the surface of a grinding wheel. The need for effective environmental control in ultra-precision grinding is emphasized by this observation; in this case to achieve continuous elimination of the loading elements at the material removal points.

Figure 4 shows two micrographs of workpiece surfaces finished with fine (a) and coarse (b) abrasive grits respectively in a set of statistical grinding experiments without ELID. Whilst a severely fractured texture can be observed in image (a), a fine surface finish and a relatively large ductile material removal area, with constant trace marks generated by abrasive grits, can be observed in image (b). One suggestion arising from the statistical analysis for conventional grinding without ELID is that the selection of a relatively coarse abrasive grit size can provide the benefit of large gaps between the abrasive grits and the workpiece surface. This could reduce subsequent deterioration of the finished surface integrity due to scratching by chips and heat generation by burnishing.

Table 3 (a) - (c) shows the results of statistical evaluation for the grinding experiments with ELID. In a comprehensive evaluation, it has become apparent that some

significant factors showed totally opposite tendencies in comparison to those observed when grinding without ELID. One of these is the advantage of applying a relatively greater depth of cut. Figure 5 shows typical examples of the workpiece surfaces finished with deeper and shallower depths of cut with coarse diamond abrasive grits and ELID, these correspond to the images (a) and (b) respectively. A sharply finished surface and a relatively large ductile material removal area, with constant trace marks generated by abrasive grits, can be observed in image (a), whilst a severely burnished surface texture appears in image (b). This tendency was thought to be associated with the selections of the feed rate and the spindle speed, which result in differences to the contact frequency of the abrasive grits. It was confirmed that the grinding environment was changed significantly with the utilization of ELID.

Furthermore, the design effect of the tooling component has also been identified as a significant factor through the ANOVA process, even when applying ELID. Statistical optimization of the grinding factors, surprisingly, shows that a tooling component with a ceramic fixture, in other words a relatively highly compliant fixture could contribute to an enhancement of surface flatness. This observation is totally opposite to the accepted maxim that extremely high rigidity in the mechanical components is crucial for achieving extremely fine surface integrity in ultra-precision machining.

Systematic statistical evaluation of the technical parameters has highlighted some key features that can be simplified to reveal the true practical material removal mode and suggest an appropriate strategy to control the material removal process. As a result of this experimental phase, a combination of statistically identified points has led to the creation of a new model for material removal in cup wheel grinding of PZT ceramics with multipoint abrasive grits.

Figure 6 summaries a general concept of this hypothesis, which is mainly associated with an advantage of applying a deeper work depth of cut. Figure 6 (a) shows schematically a material removal mode assuming a deeper work depth of cut, whilst (b) shows the effect of a shallower work depth of cut. In general, the (b) condition tends to be considered ideal for precision surface finishing of brittle materials, because this shallower depth of cut condition, which is close to the critical depth of cut, leads to ductile material removal mode at the surface. However, the statistical analysis applied here reveals the obvious tendency that this condition causes severe grain pull out of textures and deterioration of surface flatness for PZT ceramic bulks.

Additionally, through visual inspections and measurements of the finished surfaces under the deeper work depth of cut (as shown in Figure 6 (a), there is clearly a tendency for micro-fracture damage to occur at the leading (external) edge of a cup grinding wheel. Effectively this assists fine material finishing in ductile mode at the secondary material removal zone, (corresponding to the bottom of the grinding wheel), which results not only a good surface roughness, but also an excellent surface flatness. In essence, fracture damage initiated by the leading edge of the grinding wheel contributes to an effective reduction of material toughness on the PZT ceramic surface and immediate sub-surface, thereby subjecting the material to less stress concentration and less heat generation.

A unique aspect of this hypothesis is that a combination of brittle and ductile material removal is considered to be beneficial and this is because of reduction of stress concentration and heat generation at the material removal interface. This phenomenon was actually found to occur when a relatively large work depth of cut was applied. Furthermore, when worn and inclined edges are present at the external edge of the wheel bonding segment, the actual work depth of cut becomes much finer in the secondary material removal zone, and this also contributes to an enhanced surface integrity on PZT bulk ceramics.

Although the material removal model suggested here has potential applicability for other polycrystalline brittle materials, it should be noted that it is dependent on the mechanical behaviour of the workpiece material. In particular the effective fracture toughness of the grain boundaries, which may ultimately depend on material characteristics such as dislocation density and mobility, needs to fall within a certain range.

3-3. Modeling of Material Fractural Types

In the third phase of material removal analysis, an optimization of the grinding parameters was carried out for cup wheel grinding under stationary traverse mode. The trials resulted in visual categorization of the mechanical damage and fracture defects, including initial porosity. Two commonly occurring types of fracture defect were identified for surfaces ground in the deeper work depth of cut with ELID, and this has consequently led to an effective choice of grinding conditions for fine surface finishing of PZT bulk ceramics.

Figure 7 shows schematic views of the fracture types, which relate to initial porosity, namely grain pull-out and defacing, both of which are identified in the current research work. Normally, the fracture behaviour of brittle materials is discussed on the basis of well-known crack propagation modes such as median, lateral and radial cracks (Li and Liao, 1997). However, these types of crack were not observed during the investigation for PZT ceramic grinding. Instead, where the surface finish shows macroscopic damage, the tendency is towards grain pull-out (as shown in Figure 4) and random shallow peeling (defacing).

The fracture toughness of piezoelectric materials is relatively weak at the grain boundaries compared to other structural ceramics (Tanaka and Isono, 2001), and when the frequency of abrasive contacts was high, at relatively low feed-rate, it was observed in these experiments that grain pull-out became more evident. Probably this phenomenon relates to high adherence in the PZT material and weakening of the grain boundaries due to high frequency stress variation. Meanwhile, if a high feed rate is applied, assuming the same spindle revolution speed, then the theoretical amount of material removed from the workpiece surface by each of the abrasive grits is greater. This induces more severe two dimensional frictional behavior at the material removal interface. As most of the PZT ceramics exhibit a high thermal sensitivity, a combination of heat generation and adherence can be regarded as the cause of the observed surface defacing.

Through microscopic evaluation of the frequency of these two fracture types, summarized in Figure 7, optimum grinding parameters were identified for cup wheel grinding in stationary traverse mode. The optimum condition, defined with a feed rate of 5.0 mm/min, was found to produce the minimum defect density in both of the chief micro-fractural modes, ie. grain pull out and defacing. This result provides comprehensive evidence of the benefit of less contact and frictional behavior at material removal interface, and subsequently less stress variation and thermal influence on the finished surface.

Consequently, it has been confirmed that categorization of the fractural behaviour, in the manner suggested here, can be used to understand practical material removal modes, and this can be used as an effective indicator to optimize grinding conditions for polycrystalline materials such as PZT ceramics. It should be stated here that the optimized grinding condition has resulted in enhancement of surface flatness of less than 2.0 micrometer over 50 mm round PZT ceramic bulks and this reflects less variation of residual stress distribution in the subsurface area. However, the same condition leads to a slight deterioration of the surface roughness and textural integrity as a compromise (Arai, 2005).

4. Design Contribution of the Tooling Component

With respect to the contribution of machine tool components for successful material removal in ultra-precision machining, it is generally claimed that the stability of the loop distance on the machine tool structure, defined as a work depth of cut between a grinding wheel bottom surface and workpiece surface in cup grinding mode, has a critical influence on controlling the grinding forces. Thus it should be high and consistent for enhancement of surface integrity, mainly surface roughness (Slocum, 1992). Meanwhile, as described in the previous section, it has became evident through statistical evaluation of PZT ceramic grinding conditions that a relatively soft tooling device performs effectively in achieving fine surface flatness.

This tendency implies that the structural performance of both the grinding machine tool and also the tooling device is significantly associated with surface integrity control in ultra-precision machining. In fact counter-intuitive features have to be adopted occasionally so that surface roughness and flatness are optimized simultaneously. From this point of view, a machine design contribution was evaluated in the next phase of experimentation; in order to acquire practical knowledge for grinding process.

Sufficient stability of the loop distance in ultra-precision grinding can be achieved only when the overall stiffness of the machine structure is extremely high. With increased stiffness there is a tendency for the structural mass to also increase and this generally results in structures with a low resonance frequency. Perversely this can cause severe dynamic errors in the loop distance and consequently extreme deterioration of machined workpiece quality. Therefore, the balance between the structural stiffness and mass tends to be considered as the most fundamental but

significant point in the design process of machine tool structures. Consistency of the loop distance, tends to be regarded as an advanced characteristic, and there has been no clearly identified approach to cope with this factor. Although high rigidity is one of the philosophies that has been applied, it is difficult to keep structural compliance consistent at the loop distance in the wide range of dynamic excitation. Therefore, as another approach, enhancement of the damping property could potentially be used as a substitute to minimize machine-structural errors. However, high internal damping ratios usually assume a certain structural flexibility, and thus this is difficult to achieve under the restriction of a low compliance design concept. Furthermore, it is not technically easy to quantify damping characteristics as a simplified indicator on a complex machine tool structure. Therefore, the damping property of structural components and mechanical interfaces tends to be ignored on machine tool structures. If necessary certain damping elements tend to be installed as subsidiary components, such as adaptive sheets and/or hydraulic devices outside the main structural loop (Slocum, 1992).

In the series of machinability trials of PZT ceramics described above, it was occasionally observed that static and dynamic inconsistency of the loop distance, leading to variation of the grinding forces, caused a significant deterioration in the surface roughness, flatness and the textural integrity of the PZT ceramics. Since the structural stiffness could not be increased, the material removal interface between the abrasive grits and workpiece was chosen as an accessible point where enhancement of the damping property could significantly lead to improvements in the finished surface quality. Accordingly a workpiece tooling component was designed with the objective of attenuating dynamic errors in the direction of the loop distance, and the most importantly, to improve interfacial contact in the material removal zone.

Figure 8 shows a damping vacuum chuck developed for this purpose. The main part of this device, which is a hybrid tooling structure, was arranged to hold a workpiece by vacuum, with air extracted through an array of pinholes. This arrangement can give a consistently distributed suction force and minimize distortion of a PZT workpiece. The hybrid tooling structure consists of a viscoelastic polymer layer inserted between two aluminum plates. This structure has the ability to transform the dynamic energy of bending vibration modes into frictional energy inside the viscoelastic polymer layer, and hence to effectively absorb the mechanical vibration. When the two aluminum plates vibrate in the same bending mode, the viscoelastic polymer layer between them expands and shrinks in-plane. Since the polymeric layer consists of long chain molecules, respective motion of each molecule causes microscopic friction and this phenomenon results in heat generation. In practice, this form of energy dissipation can typically be expected only when the hybrid tooling structure deforms in bending modes.

Under static conditions, the bending stiffness of the hybrid tooling structure is less than that of an aluminum solid plate whose dimensions are the same as those of the hybrid tooling structure. This feature gives a flexible acceptance at the material removal interface and a stable, in other words averaged, internal stress distribution inside the workpiece in practical grinding. Although serial installation of soft components into the structural loop directly between a tool and workpiece is rare due

to the lack of rigidity, both attenuation of dynamic errors and consistency of stress distribution inside the workpiece are expected in this case.

The viscoelastic material used was an acrylic polymer whose thickness is less than 1.0 mm. This material has the particular dynamic response that high frequency excitation induces high stiffness. As with most polymers stiffness is also temperature dependent. Hence if grinding forces vary in the high frequency range, the structural stiffness becomes high. In other words, the actual mechanical characteristics of the hybrid tooling structure respond dynamically to variations in the grinding forces.

In the final phase of experimentation the performance of hybrid tooling structures was studied, with various different polymer layer thicknesses, in order to evaluate the general effect of the suggested strategy on surface integrity for PZT ceramics.

Figure 9 (a) – (c) shows plots of general performance data with regard to several hybrid tooling structures with different viscoelastic polymer thicknesses (50.8, 127, 254 and 508 microns). The dynamic behavior was modeled using numerical simulations and it was verified through experimental modal analysis of the hybrid tooling structures (subsequently followed by grinding experiments). It became apparent that each hybrid tooling structure has a different resonance frequency directly related to the thickness variation of viscoelastic polymer layer. Energy dissipation was obtained, although the real damping performance was attenuated due to a lack of stiffness in the support elements of the hybrid tooling structure.

Meanwhile, it was revealed after grinding trials that these tooling devices improve the finished surface integrity dramatically. Optical quality being obtained on the ground workpieces. Typical examples are shown in Figure 10 (a) - (d). These results clearly show that the tooling device can dissipate the energy of the structural bending vibrations significantly at the material removal interface in practical grinding. The surface flatness obtained in the grinding experiments was also improved with the installation of the hybrid tooling structure, and this implies that quasi-static soft contact manner at the material removal points enhances the consistency of grinding forces to give a stable stress distribution, and the most importantly, less fractural damage on workpiece surfaces.

A series of ceramic samples, produced under the optimized grinding condition, showed that a balance of structural stiffness and acceptance, in other words, an accuracy guaranteed by the machine structure and appropriate flexibility which compensates for static and dynamic error modes at the material removal interface, is significant in successful ultra-precision grinding of PZT ceramics. Figure 11 shows the general concept of this idea, which emphasizes the advantage of the soft contact strategy.

5. Conclusion

Material removal mechanisms in practical ultra-precision grinding of PZT ceramics and the effect of the tooling component were investigated interactively in order to determine the conditions required for consistently high quality of surface roughness, surface flatness with minimum fractural damage.

In the first machinability trials, microscopic fractural modes were investigated. This revealed that native porosity in the bulk shows certain networks that are associated with the sintering process. During machining, these defects become the origins of dislocation and crack propagation, which are assisted significantly by relatively low boundary toughness between the polycrystalline textures.

By applying statistical methods the key technical factors were defined for successful ultra-precision grinding of PZT ceramics. This was achieved through comprehensive evaluation of the tendencies revealed by the analysis of variance (ANOVA) and a series of discussions has subsequently led to the establishment of a unique material removal model for multi-point practical grinding of PZT ceramics. It should be noted that the statistical evaluation considers not only grinding parameters and material properties, but also design characteristics of tooling devices and furthermore interactions of technically defined factors, assuming the material removal manner as a systematic phenomenon.

During the experimental optimization of the grinding parameters, defects induced on the ground surfaces were categorized, and the frequency of each type on the finished surfaces was assessed. This methodology has provided a good explanation for the visual evidence, and a recommendation for the grinding parameters needed to guarantee excellent surface roughness and flatness on PZT bulk ceramics.

In the final phase of investigation, the contribution of a tooling component was discussed, and then this has led to the development of a hybrid tooling device which aims to appropriately control the manner of contact at the material removal interface. In a departure from conventional thinking, a vacuum chuck with a viscoelastic polymer interlayer was developed. This was found to enhance damping characteristics and hence consistency of the stress distribution during the grinding process. Consequently, it became apparent that the tooling device performs effectively to give drastic improvement of ground surface integrity and this was verified by experimentation.

Through all of the discussions, it has been theoretically and experimentally confirmed that successful surface integrity control in practical ultra-precision grinding can be achieved only when the interface condition between the abrasive grits and the workpiece surface is appropriately controlled. The soft contact approach, which has been discussed mainly in relation to tooling development, can provide a major breakthrough for surface integrity control of brittle materials by ultra-precision grinding.

6. Acknowledgements

The authors would like to thank the NSK Ltd. for its financial support under the overseas research program.

7. References

Arai, S., Corbett, J., Whatmore, R.W., Wilson, S.A, Hedge, J., 2004. *Surface Integrity Control of Piezoelectric Materials in Ultra Precision Grinding - Based on Tooling Design Analysis*. Conference Proceedings, 4th International Conference & 6th Annual General Meeting of the European Society for Precision Engineering and Nanotechnology, Glasgow, 201-202.

Arai, S., 2005. *Surface Integrity Control of Piezoelectric Materials in Ultra Precision Grinding on the basis of Machine Design Assessment* ; PhD Thesis, Cranfield University.

Beltrao, P.A., Corbett, J., Gee, A.E., Whatmore, A.E., Goat, C.A., Impey, S.A., 1997. *Diamond Machining of Ferroelectric Materials.* Proceedings of the 9th International Precision Engineering Seminar & 4th International Conference on Ultraprecision in Manufacturing Engineering, Progress in Precision Engineering and Nanotechnology, Braunschweig Germany, May 26th –30th 2, 578-581.

Beltrao, P.A., 1998. *Analysis of the Potential for Ductile Mode Machining of Ferroelectric Ceramic Materials*. PhD Thesis, Cranfield University.

Bifano, T.G., Dow, T.A., Scattergood, R.O., 1998. *Ductile-Regime Grinding of Brittle Material*. UPT - Ultraprecision in Manufacturing Engineering. Proceedings of the International Congress for Ultraprecision Technology, Aachen. FRG Springer-Verlag, 22-40.

Corbett, J., Stephenson, D.J., Sweet, J., Wills-Moren, W.J., 1999. *An Ultra Precision Machine Tool Demonstrating a Novel Vibration Resistant Structure*. Proceedings of the euspen 1st International Conference & General Meeting of the European Society for Precision Engineering and Nanotechnology, Bremen 1 159-162.

Corbett, J., Mckeown, P.A., Peggs, G.A., Whatmore, R.W., 2000. *Nanotechnology: International Developments and Emerging Products*. Annals of the CIRP Keynote Papers 49 2 523-545.

Corbett, J., 2001a. *Diamond Micromachining, in:* McGepugh, J. (Ed.), Micromachining of Engineering Materials. Marcel Dekker Inc. New York, pp. 125-146.

Corbett, J., Stephenson, D.J., 2001b. *The Control of Surface Integrity by Precision Machining and Machine Design.* Proceedings of International Congress of Precision Machining - ICPM 2001, 31-42.

Desa, O., Bahadur, S., 1999. *Material Removal Mechanism and Subsurface Damage Studies in Dry and Lubricated Single-Point Scratch Tests on Alumina and Silicon Nitride*. Wear 225–229 1264-1275.

Editorial Office of Tool Engineers, 1990. *Utilization Manual for Grinding Machines*. Taiga Publications, Tokyo [in Japanese].

Encyclopedia of New Machining Tools, 1991. Sangyo-Chosa-Kai, Tokyo [in Japanese].

Fan, H., Keer, L.M., Cheng, W., Cheng, H.S., 1993. *Competition Between Fatigue Crack Propagation and Wear*. Transactions of the ASME Journal of Tribology 115 January 141-147.

Griffiths, B., 2001. *Manufacturing Engineering Modular Series: Manufacturing Surface Technology, Surface Integrity & Functional Performance* Penton Press, Cleveland, Ohio.

Inasaki, I., 1987. *Grinding of Hard and Brittle Materials*. Annals of the CIRP 36 2 463-471.

Inasaki, I., 2004. *Machining Processes in Precision Engineering*. in: Klocke, F., Pritschow, G. (Eds.), Autonome Produktion. Springer, New York, pp. 27-37.

Kanai, A., Miyashita, M., Sato, M., Daito, M., 1995. *Proposal of High Productivity in Ductile Mode Grinding of Brittle Materials*. American Society for Precision Engineering, Proceedings 12 167-170.

Klocke, F., Hambucker, S., 1997. *Technology and Model Development for Ductile Grinding of Optical Glass.* Proceedings of the 9th International Precision Engineering Seminar & 4th International Conference on Ultraprecision in Manufacturing Engineering, Progress in Precision Engineering and Nanotechnology, Braunschweig Germany, May 26th –30th 2 513-516.

Li, K., Liao, W., 1997. *Modelling of Ceramic Grinding Process, Part I, Number of Cutting Points and Grinding Forces per Grit*. Journal of Material Processing Technology 65 1-10.

Malkin, S., Hwang, T.W., 1996. *Grinding Mechanisms for Ceramics*. Annals of the CIRP 45 2 569-580.

McKeown, P.A., Corbett, J., 2004. *Ultra Precision Machine Tools*, in: Klocke, F., Pritschow, G. (Eds.), Autonome Produktion. Springer, New York, pp. 313-327.

Marshall, D.B., Evans, A.G., Khuri Yakub, B.T., Tien, J.W., Kino, G.S., 1983. *The Nature of Machining Damage in Brittle Materials*. Proceedings of the Royal Society of London A 385 461-475.

Morgan Matroc Ltd., Transducer Products Division, 2002. *Piezoelectric Ceramics Data Book for Designers*.

Setter, N., 2001. *Electroceramics: looking ahead*. Journal of the European Ceramic Society 21, 1279-1293.

Slocum, A.H., 1992. *Precision Machine Design*. Prentice Hall Inc., New Jersey.

Stephenson, D.J., Veselovac, D., Manley, S., Corbett, J., 2001. *Ultra Precision Grinding of Hard Steels.* Journal of International Societies for Precision Engineering and Nanotechnology 25 336-345.

Tanaka, T., Isono, Y., 2001. *A Study of Ductile / Brittle Modes Grinding of PZT Ceramics*. Journal of the Society of Grinding Engineers 45, No.8 391-396 [in Japanese].

Uchino, K., 2004. *Piezoelectric Actuators 2004 – Materials, Design, Drive/Control, Modeling and Applications.* Proceedings of ACTUATOR 2004 9th International Conference on New Actuators 14-16th June 2004 Bremen Germany. 38-47.

Uchino, K., 2006. *Piezoelectric Actuators 2006 – Expansion from IT/Robotics to Ecological/Energy Applications.* Proceedings of ACTUATOR 2006 10th International Conference on New Actuators 14-16th June 2006 Bremen Germany. 48-57.

Warnecke, G., Barth, C., 1999. *Optimization of the Dynamic Behavior of Grinding Wheels for Grinding of Hard and Brittle Materials Using the Finite Element Method*. Annals of the CIRP 48 1 261-264.

Wilson, S.A., Jourdain, R. P-J., Whatmore, R. W., Morantz, P., Corbett, J., Hucker, M.J., Warsop, C., 2006. *Ultra-precision machining of 30 micron PZT-on-silicon laminates for piezoelectric MEMS.* Proceedings of ACTUATOR 2006 10th International Conference on New Actuators 14-16th June 2006 Bremen Germany 748-751.

Wilson, S.A. and Bowen C.R. Eds., 2007. *New Materials for Micro-scale Sensors and Actuators – An Engineering Review*. Materials Science and Engineering Reports – R 56 Issues 1-6 1-129

Zhang, B., Zheng, X.L., Tokura, H., Yoshikawa, M., 2003. *Grinding Induced Damage in Ceramics*. Journal of Materials Processing Technology 132 353-364.

Figure and Table Legends

Figure 1 Microscopic optical image of PZT ceramic surface
a) Direct optical image of a polished surface, illuminated vertically
b) Background optical image of a polished surface, scattered reflection obtained with inclined illumination

Figure 2 Cracked PZT ceramic showing a circular trace mark from grinding – Ferroperm PZ26, 4500rpm, 5mm/min feed rate, 5 micron depth-of-cut

Figure 3 Schematic model of material removal behavior without ELID
a) Ideal material removal with abrasive grits
b) Detected material removal with abrasive grits and loading elements

Figure 4 Surface quality finished with different abrasive grits - Ferroperm PZ26, 2000rpm, 6mm/min feed rate, 5 micron depth-of-cut, aluminium vacuum chuck, gaseous secondary electron images
a) Surface ground with fine abrasive grits / 3-6 microns
b) Surface ground with fine abrasive grits / 6-12 microns

Figure 5 Surface quality finished with different depth of cut and ELID – Ferroperm PZ26, 6000rpm, 6-12 microns grit, 5mm/min feed rate, gaseous secondary electron images
a) Depth of cut 5 microns
b) Depth of cut 0.5 microns

Figure 6 Material removal model on the basis of statistical analysis
a) With deep work depth of cut
b) With shallow work depth of cut

Figure 7 Material fractural types and frequency. Grain pull-out – left; defacing - right

Figure 8 Damping vacuum chuck

Figure 9 General performance of hybrid tooling structure
a) Angular frequency ratio
b) Loss factor
c) Finished surface roughness and flatess

Figure 10 Optical quality of ground PZT ceramic circular discs – Ferroperm PZ26 with damping chuck
a) left - 5mm/min, 1500 rpm (51 nm Ra), right – 15mm/min, 1500rpm (58.1nm Ra)
b) left - 1mm/min, 1500 rpm (49.2 nm Ra), right – 5mm/min, 6000rpm (25.1nm Ra)

Figure 11 Balance of Rigidity and Soft Contact

Table 1 Parameter array for statistical grinding experiments

Table 2 Results of Statistical Evaluation / without ELID
a) Analysis of variance for surface roughness
b) Analysis of variance for surface flatness
c) Analysis of variance for textural damage

Table 3 Results of Statistical Evaluation with ELID
a) Analysis of variance for surface roughness
b) Analysis of variance for surface flatness
c) Analysis of variance for textural damage

Figure 1a

Click here to download high resolution image

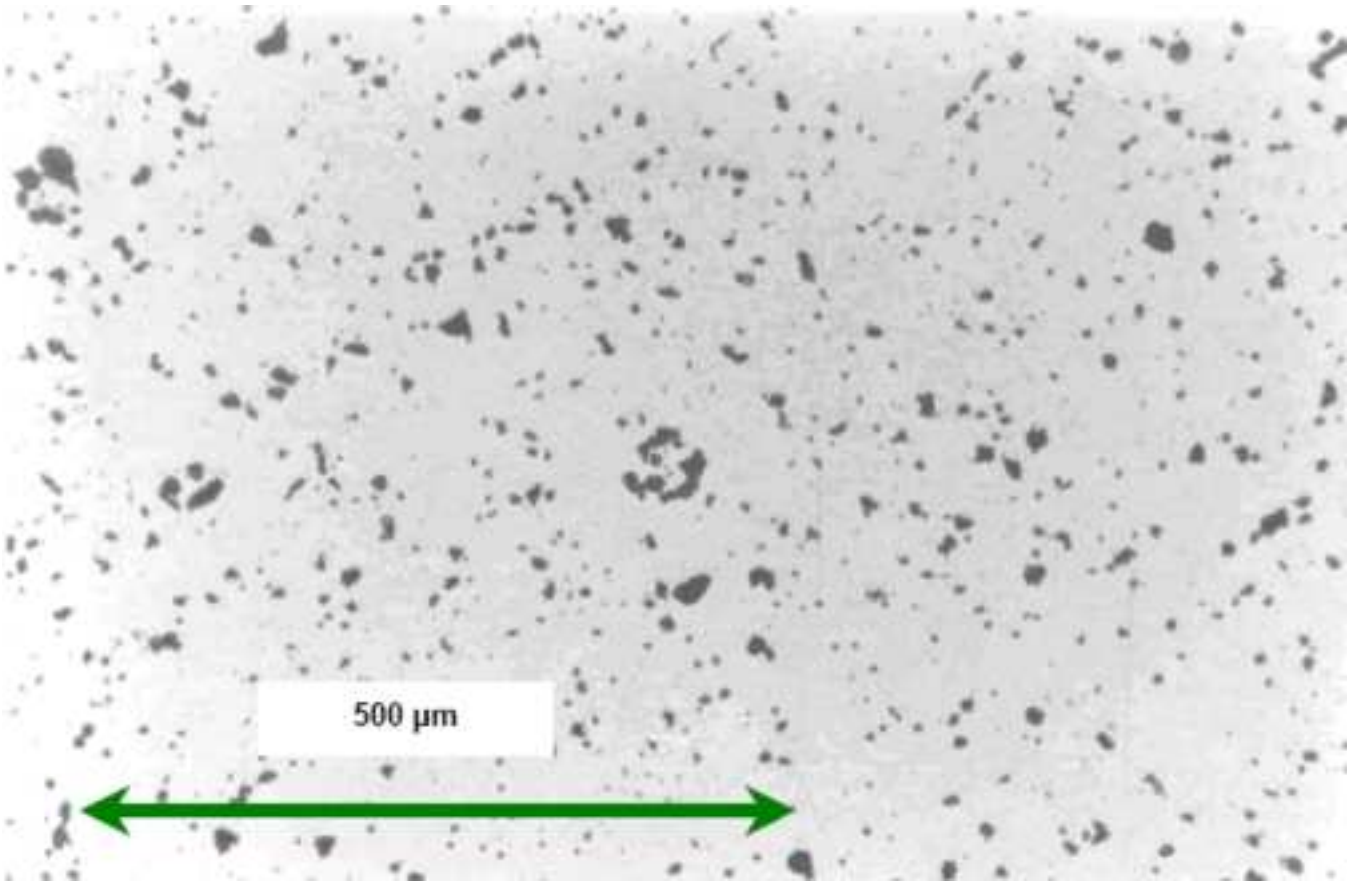

Figure 1b

Click here to download high resolution image

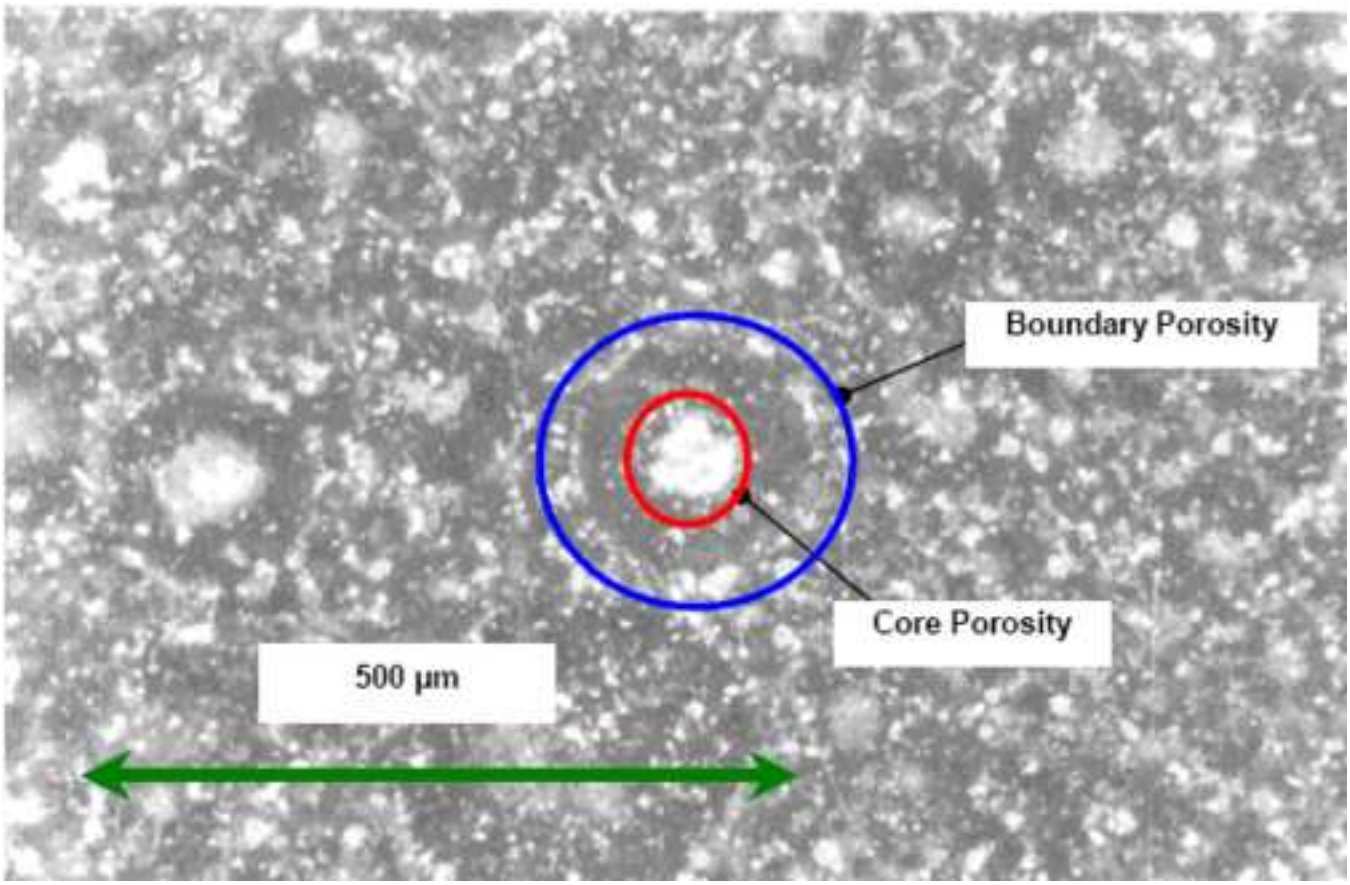

Figure 2

Click here to download high resolution image

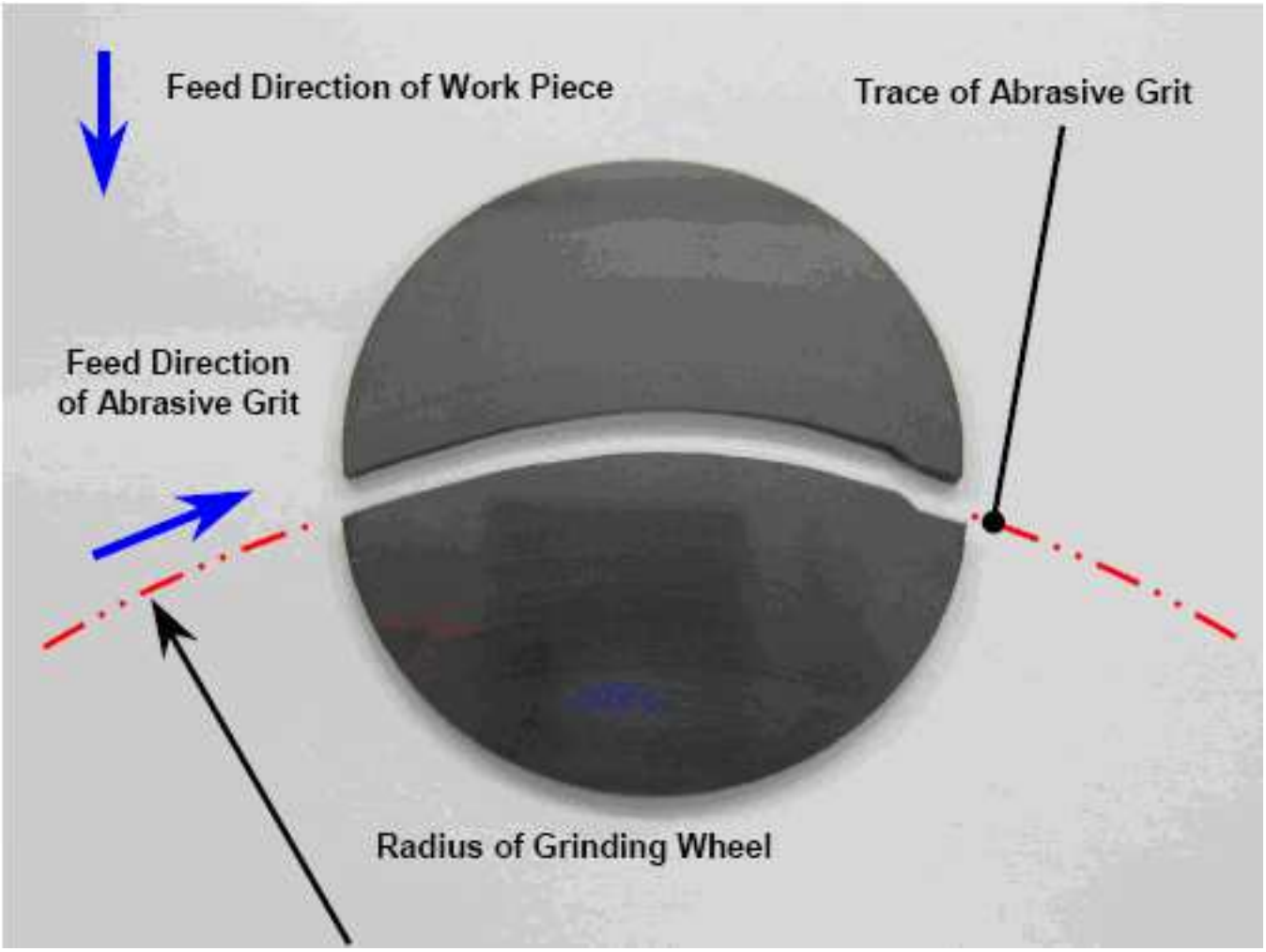

Figure 3a
Click here to download high resolution image

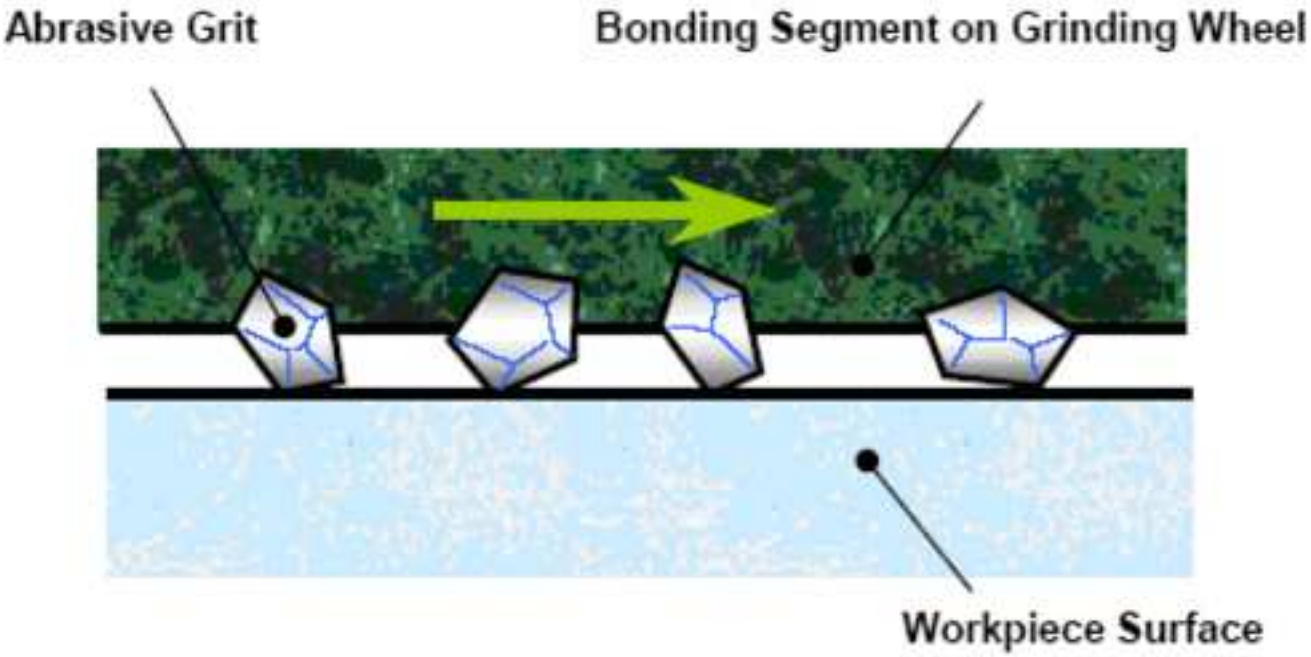

Figure 3b

Click here to download high resolution image

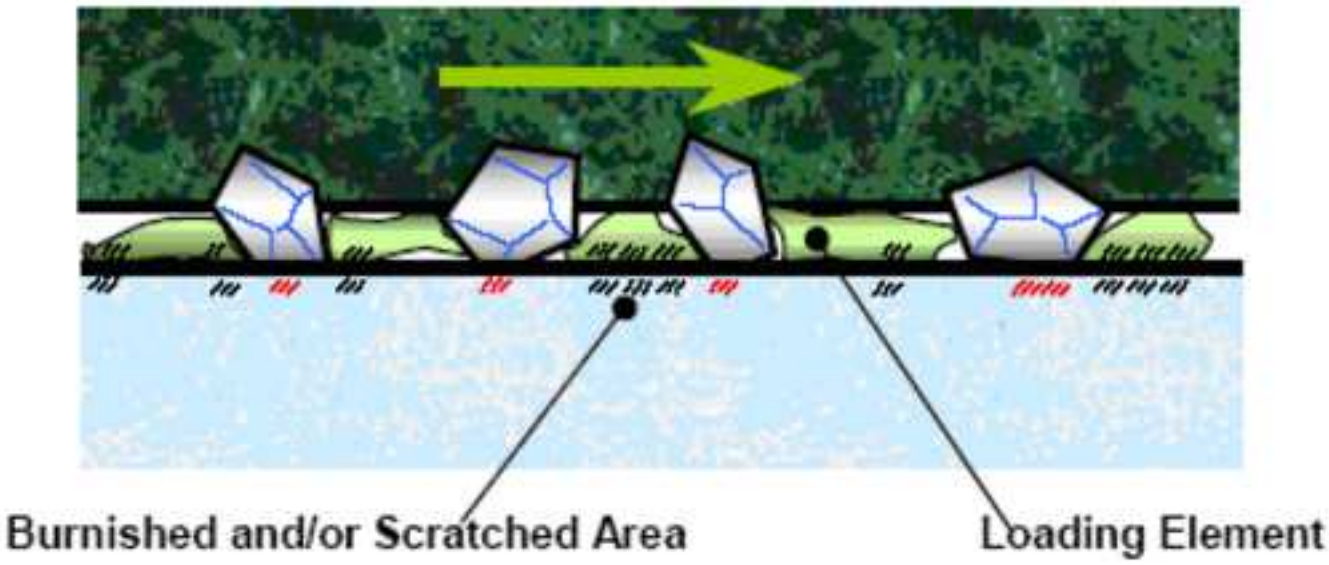

Figure 4a

Click here to download high resolution image

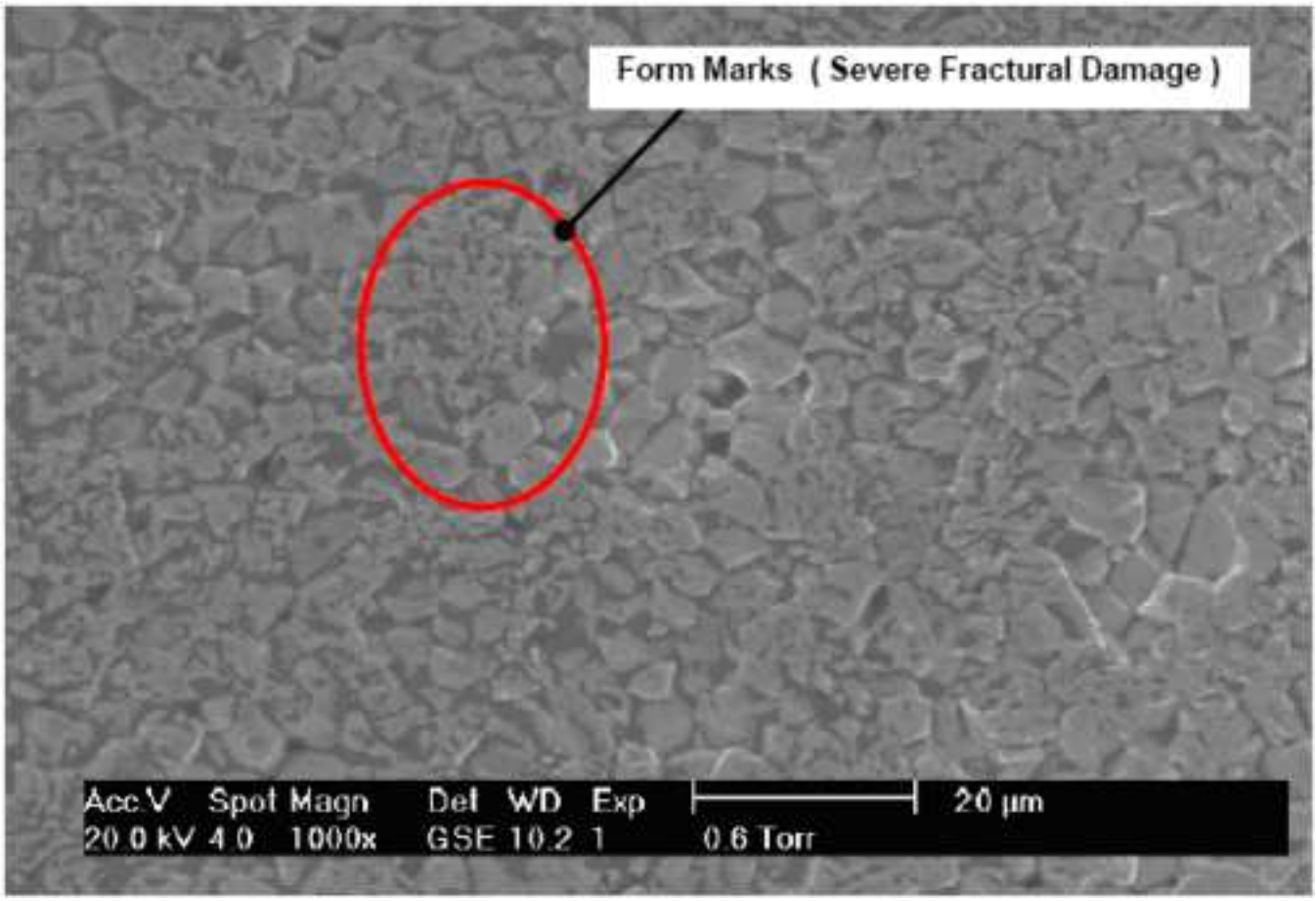

Figure 4b

Click here to download high resolution image

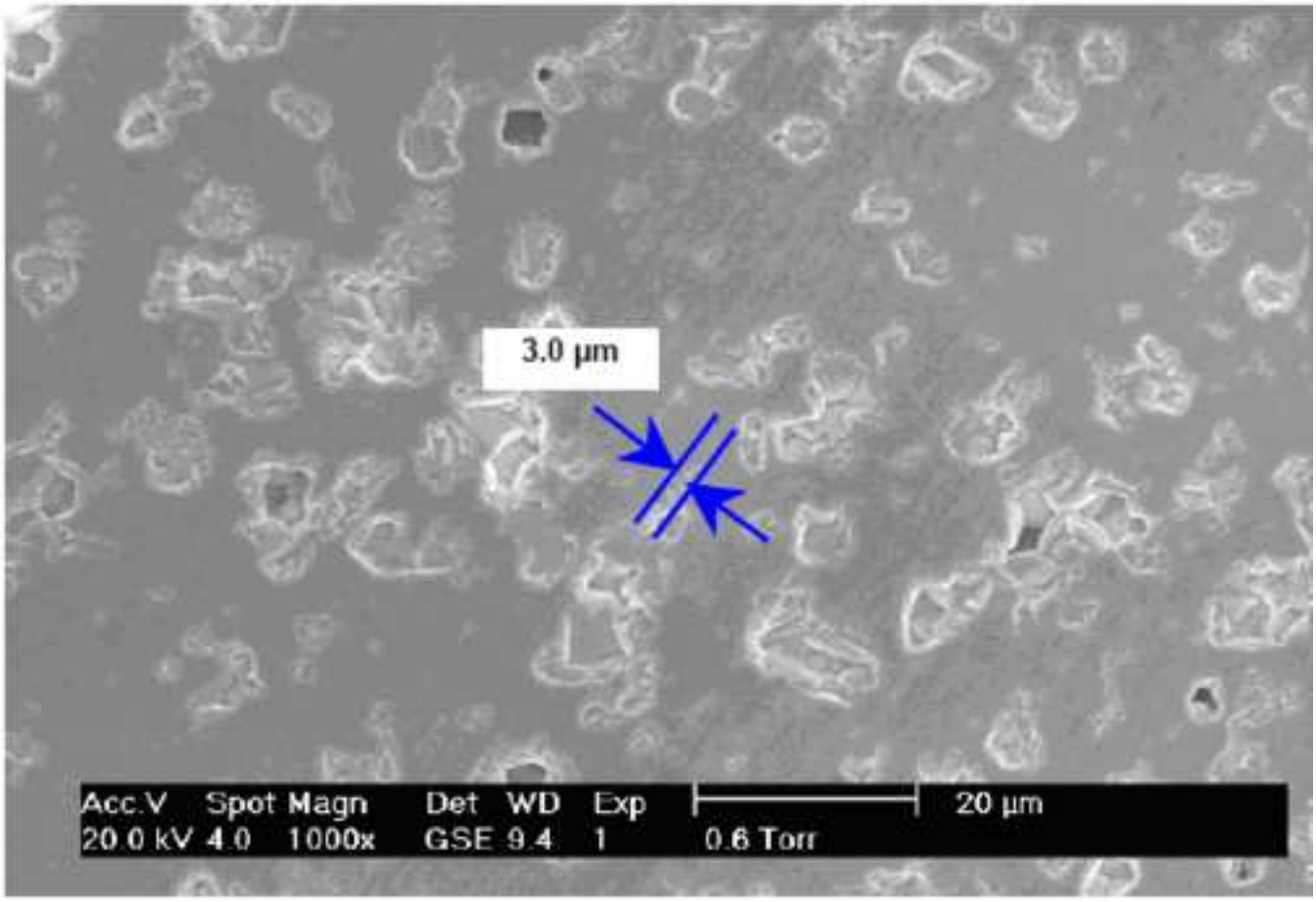

Figure 5a

Click here to download high resolution image

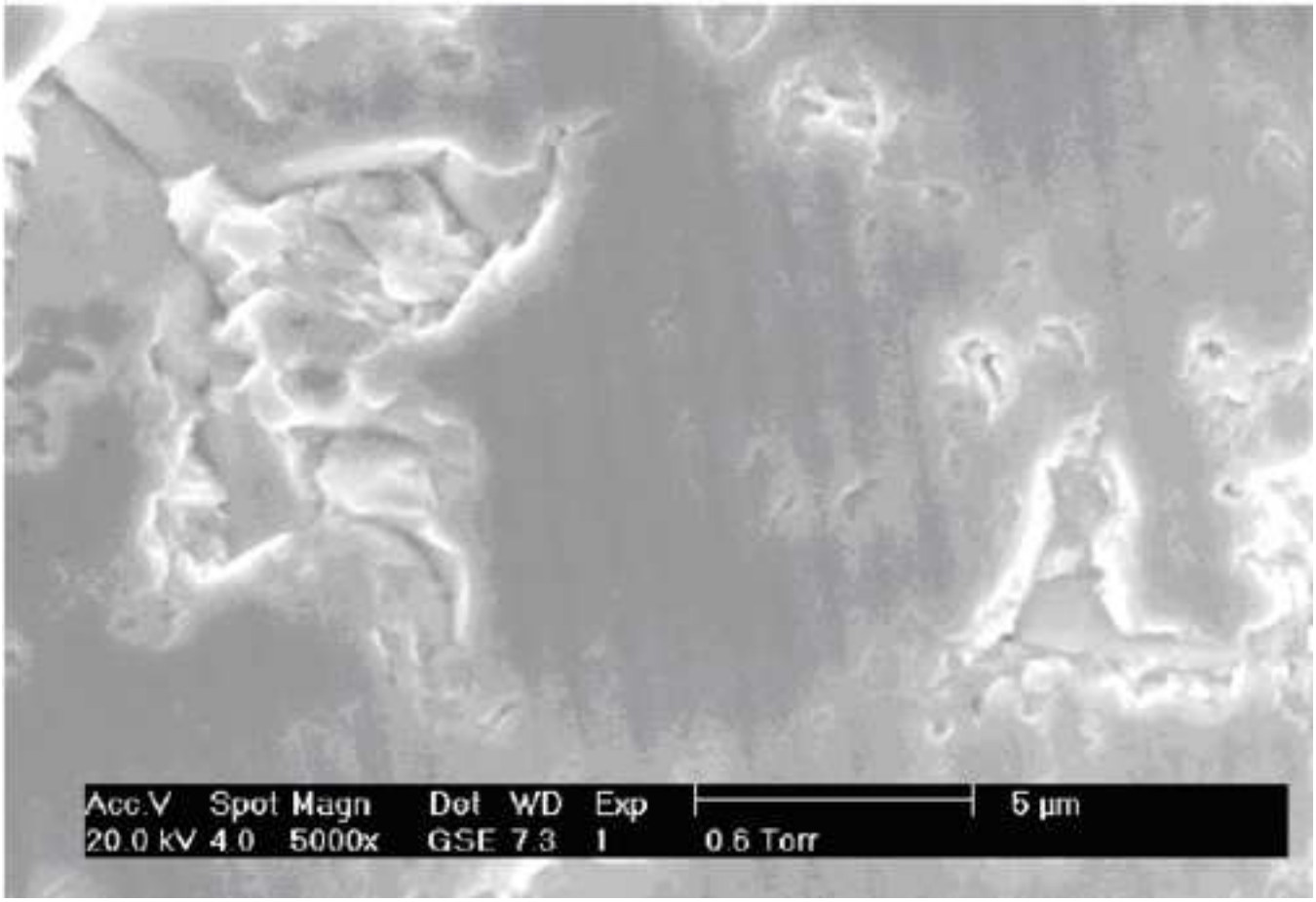

Figure 5b

Click here to download high resolution image

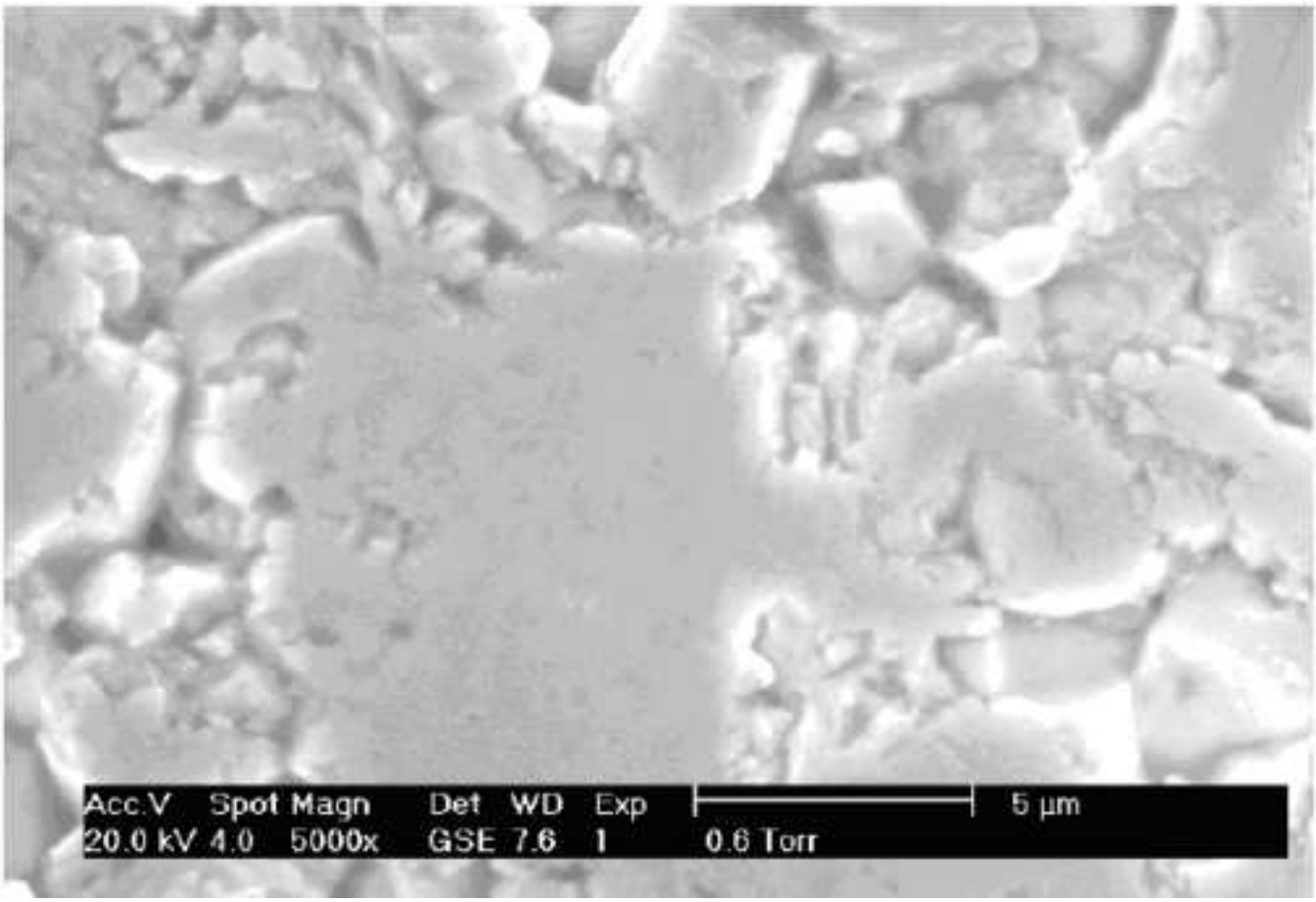

Figure 6a

Click here to download high resolution image

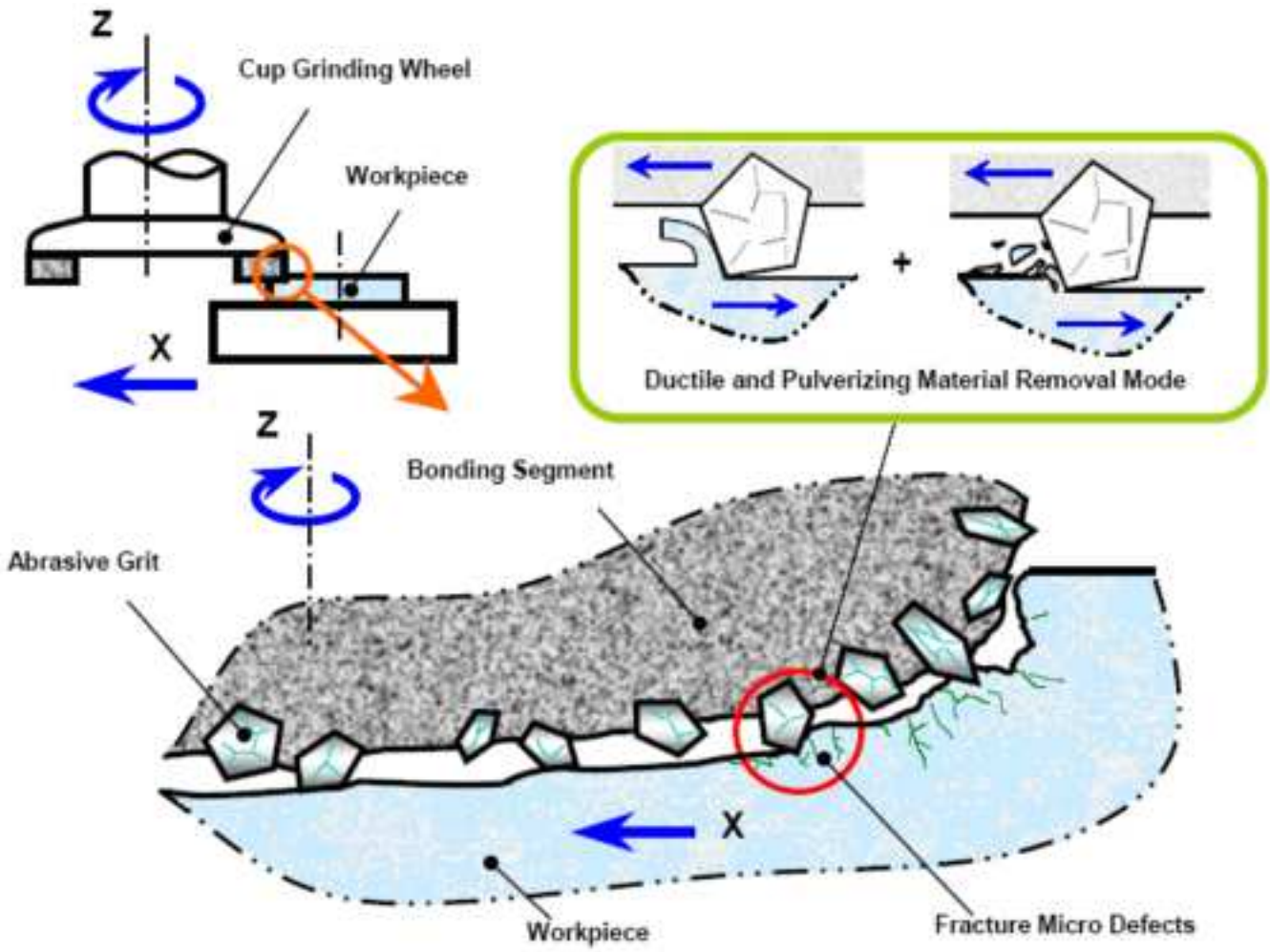

Figure 6b

Click here to download high resolution image

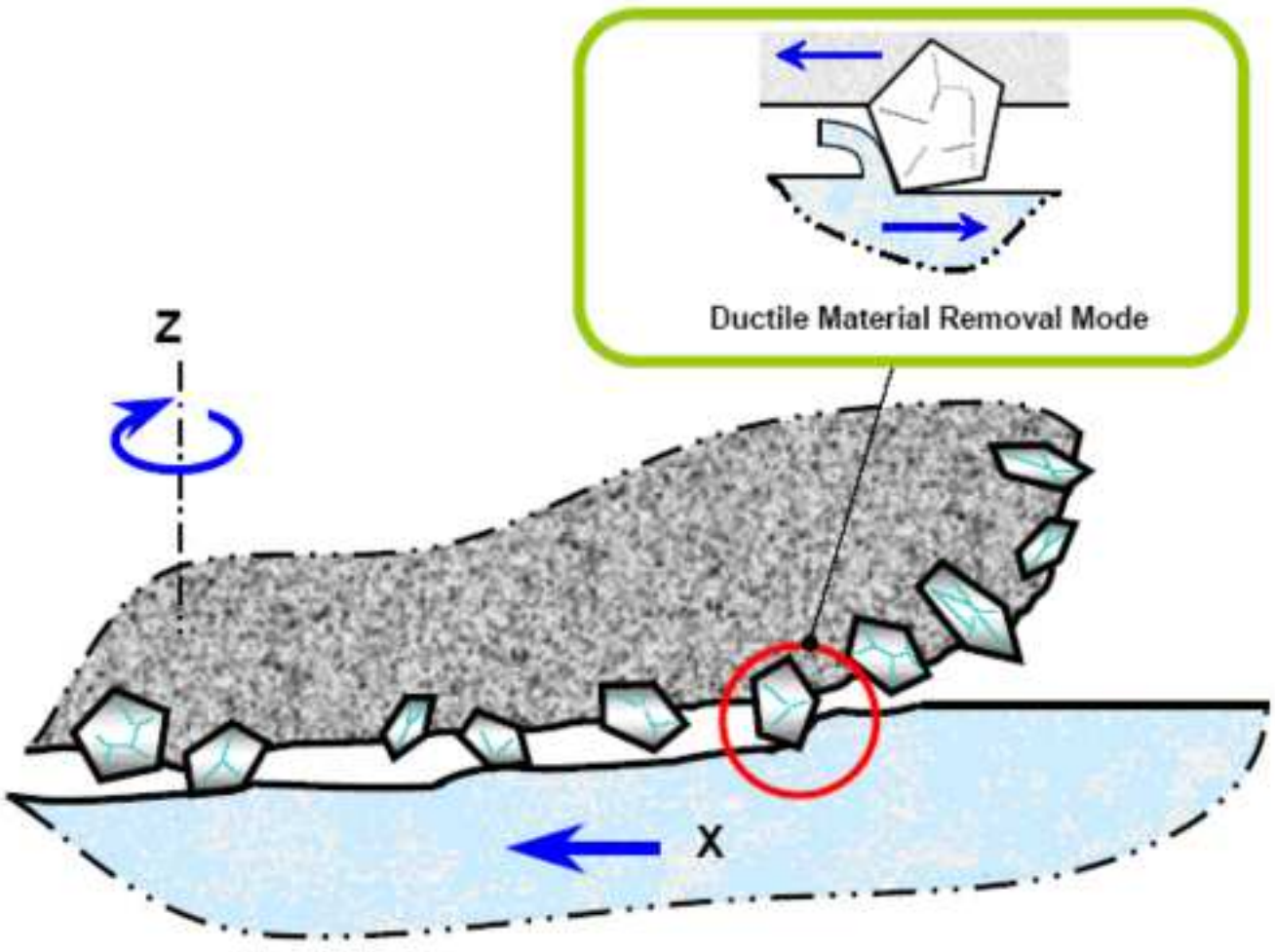

Figure 7

Click here to download high resolution image

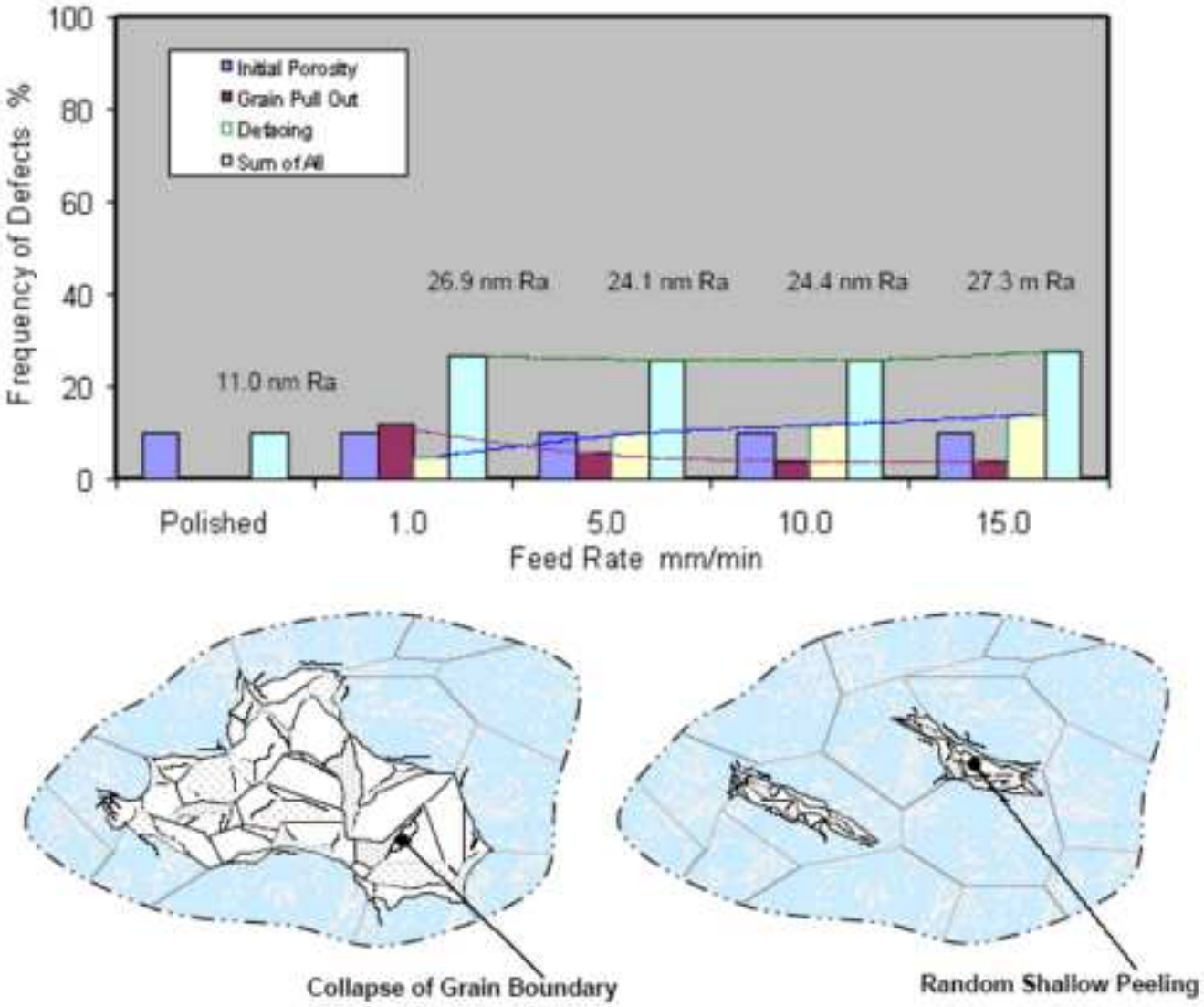

Figure 8

Click here to download high resolution image

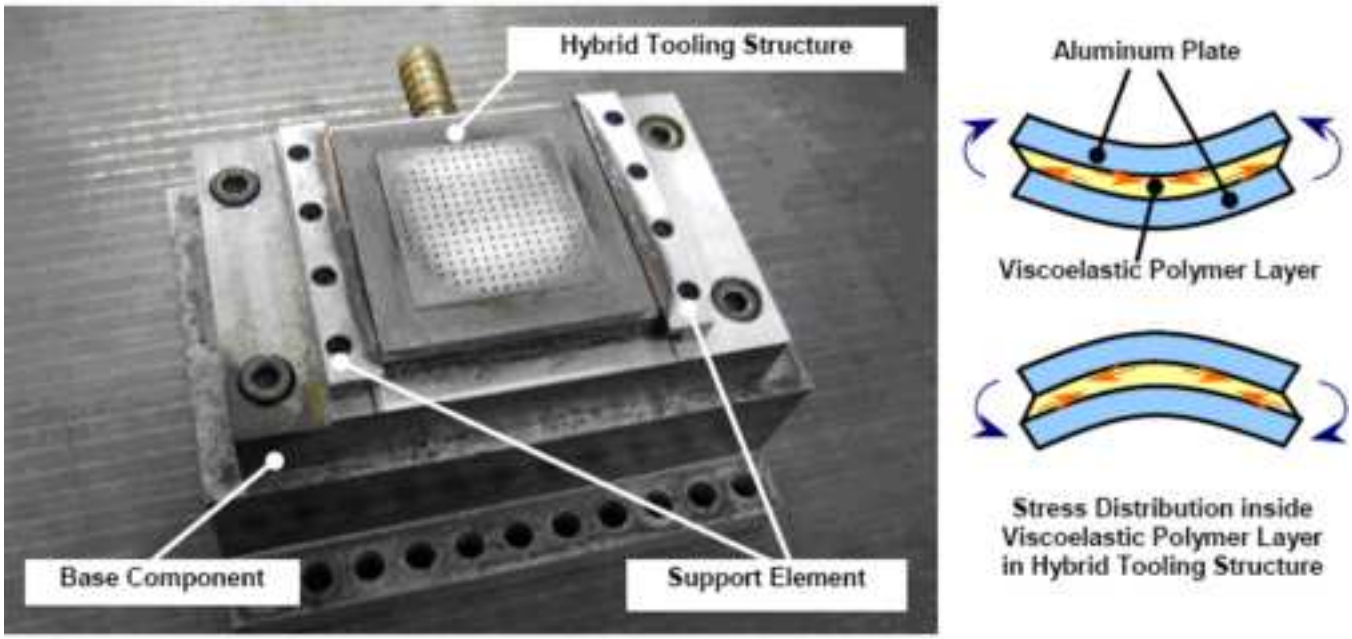

Figure 9a

Click here to download high resolution image

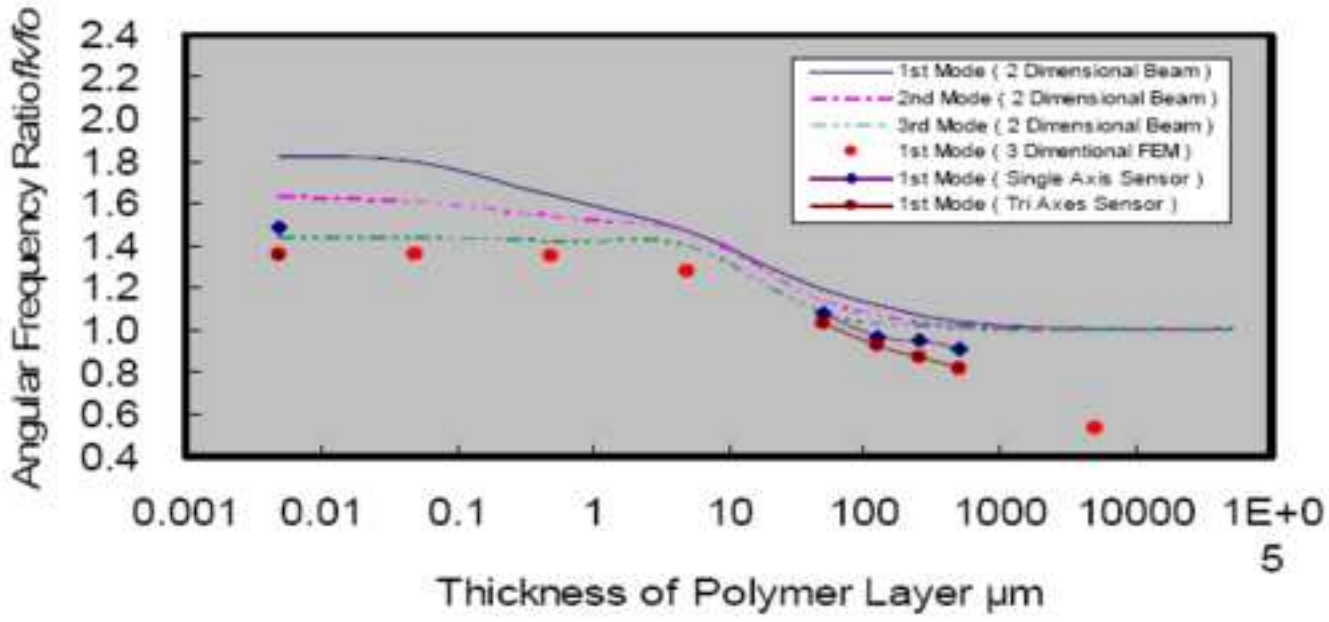

Figure 9b

Click here to download high resolution image

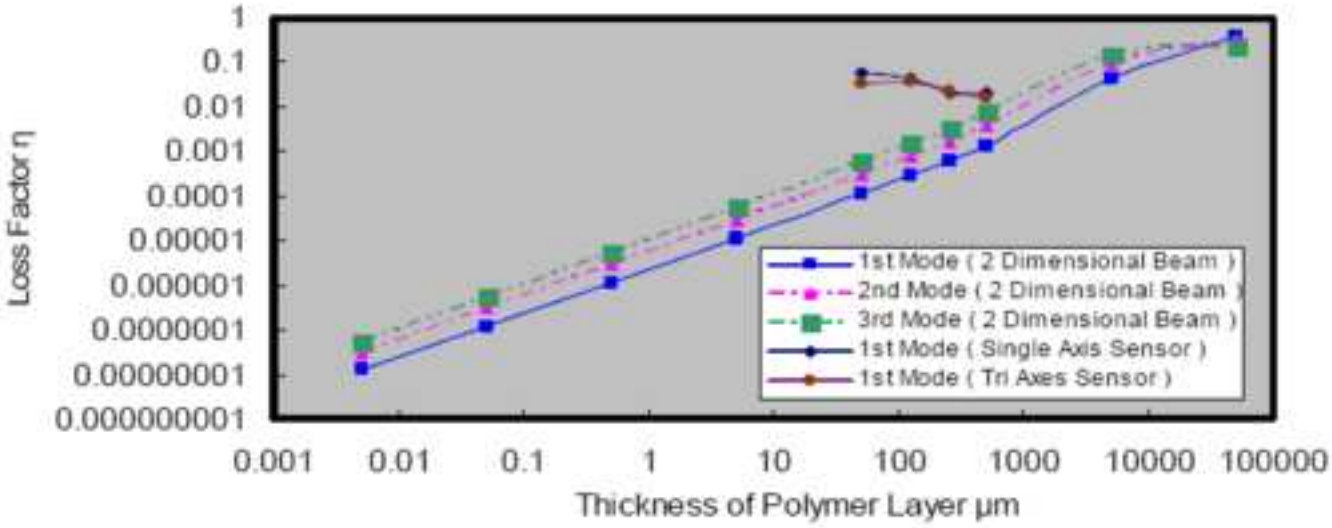

Figure 9c

Click here to download high resolution image

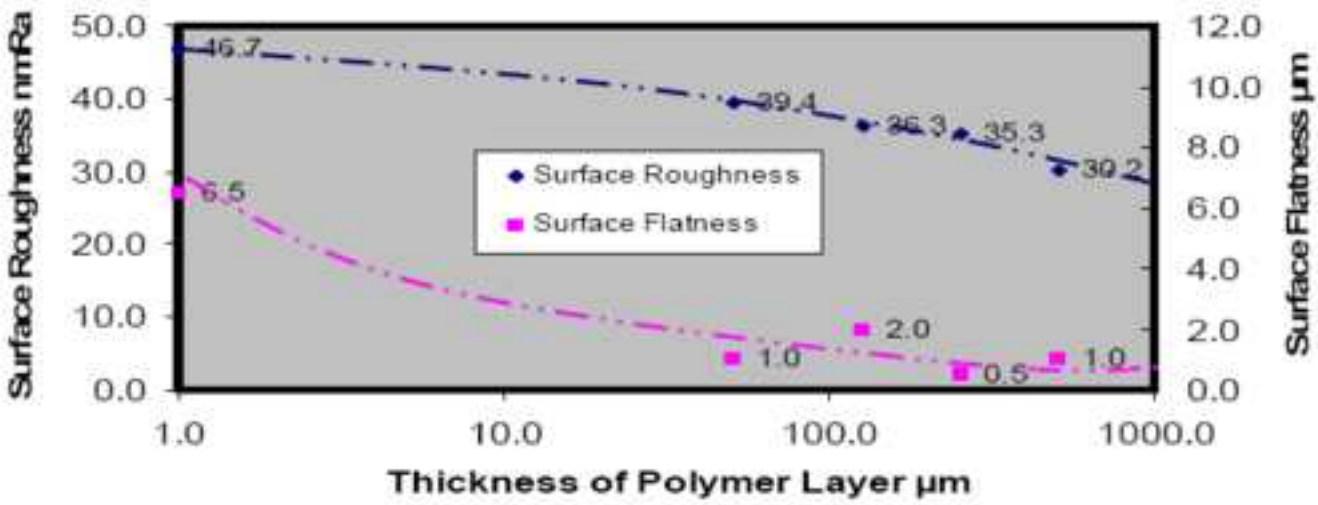

Figure 10a
Click here to download high resolution image

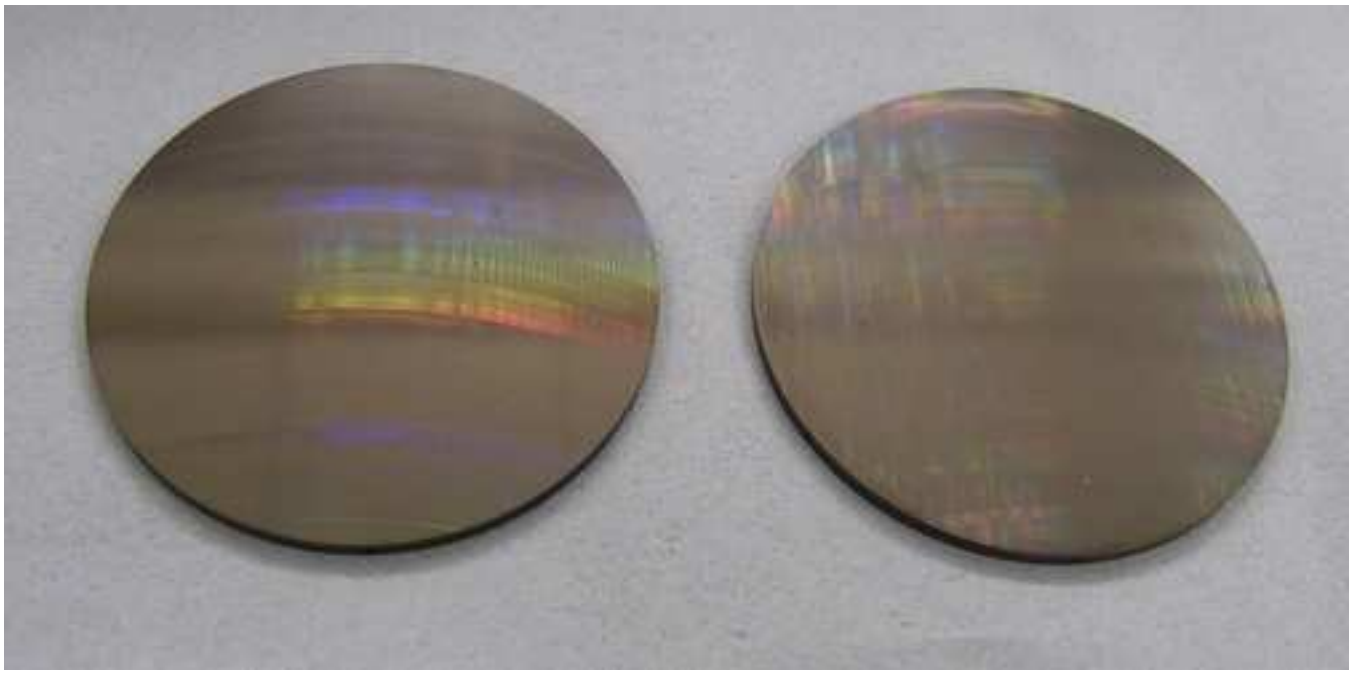

Figure 10b

Click here to download high resolution image

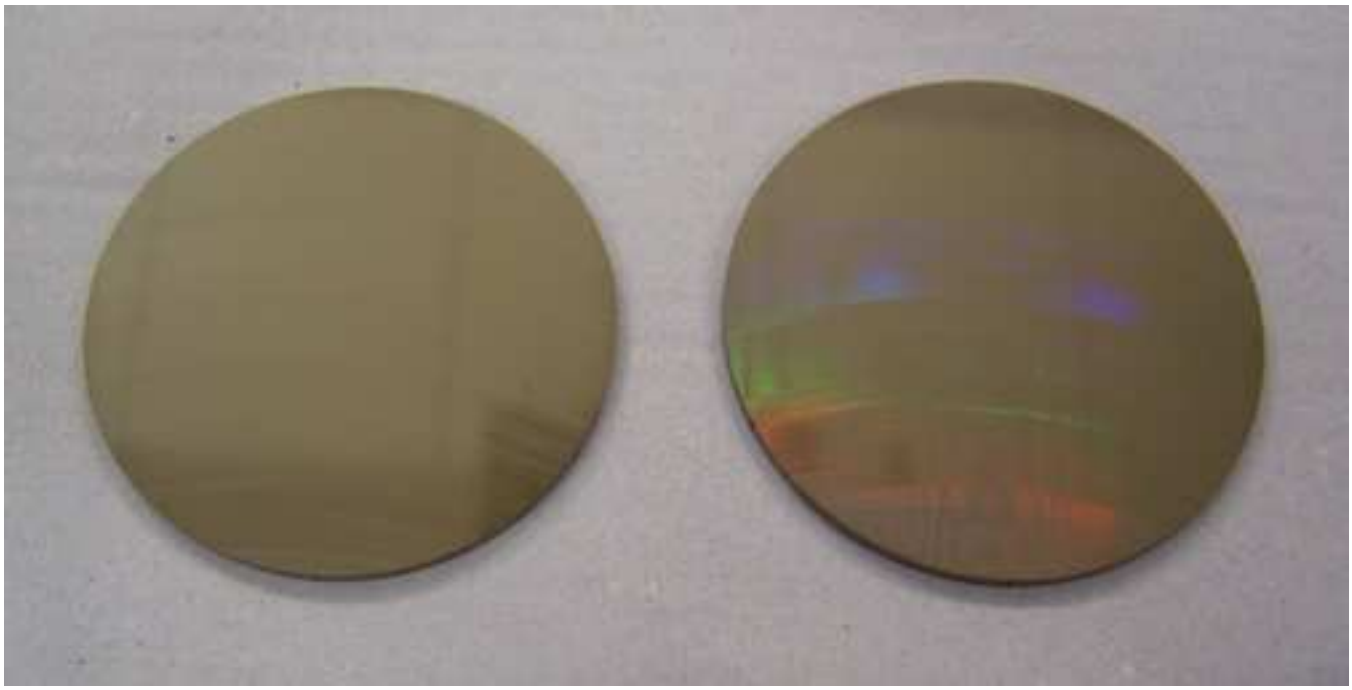

Figure 11

Click here to download high resolution image

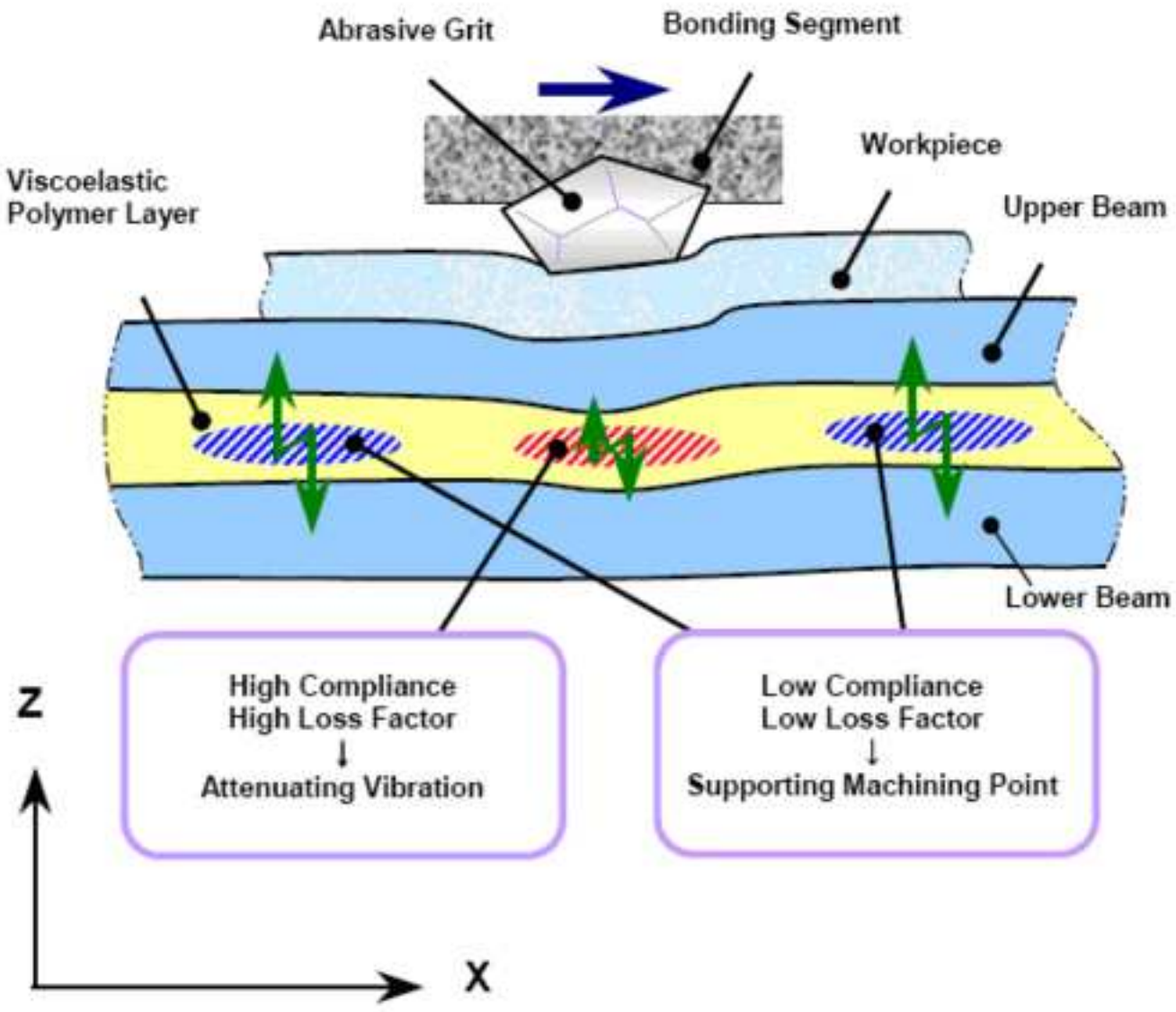

Table 1

Click here to download high resolution image

Run No.	Feed Rate mm/min	Spindle Speed rpm	A×B	Material	A×C	B×C	A×B×C	Abrasive Grit Size μm	A×D	Work Depth of Cut μm	A×B×D	Vacuum Chuck	A×G	C×F	A×B×G
1	1.0	2000	+	PZ26	+	+	+	3 ~ 6	+	0.5	+	Al	+	+	+
2	1.0	2000	+	PZ26	+	+	+	6 ~ 12	-	5.0	-	Ceramic	-	-	-
3	1.0	3000	+	PZ27	-	-	-	3 ~ 6	+	0.5	+	Ceramic	-	-	-
4	1.0	2000	+	PZ27	-	-	-	6 ~ 12	-	5.0	-	Al	+	+	+
5	1.0	6000	-	PZ26	+	-	-	3 ~ 6	+	5.0	-	Al	+	-	-
6	1.0	6000	-	PZ26	+	-	-	6 ~ 12	-	0.5	+	Ceramic	-	+	+
7	1.0	6000	-	PZ27	-	+	+	3 ~ 6	+	5.0	-	Ceramic	-	+	+
8	1.0	6000	-	PZ27	-	+	+	6 ~ 12	-	0.5	+	Al	+	-	-
9	6.0	2000	-	PZ26	-	+	-	3 ~ 6	-	0.5	-	Al	-	+	-
10	6.0	2000	-	PZ26	-	+	-	6 ~ 12	+	5.0	+	Ceramic	+	-	+
11	6.0	2000	-	PZ27	+	-	+	3 ~ 6	-	0.5	-	Ceramic	+	-	+
12	6.0	2000	-	PZ27	+	-	+	6 ~ 12	+	5.0	+	Al	-	+	-
13	6.0	6000	+	PZ26	-	-	+	3 ~ 6	-	5.0	+	Al	-	-	+
14	6.0	6000	+	PZ26	-	-	+	6 ~ 12	+	0.5	-	Ceramic	+	+	-
15	6.0	6000	+	PZ27	+	+	-	3 ~ 6	-	5.0	+	Ceramic	+	+	-
16	6.0	6000	+	PZ27	+	+	-	6 ~ 12	+	0.5	-	Al	-	-	+
Ref.	A	B	A×B	C	A×C	B×C	A×B×C	D	A×D	F	A×B×D	G	A×G	C×F	A×B×G
	1	2	3	4	5	6	7	8	9	10	11	12	13	14	15

Level of Factors : ▭ / Level 1, ▭ / Level 2

Table 2a

Click here to download high resolution image

Factor		S	ϕ	V	F_0	$F(\alpha,\phi,0.05)$	$F(\alpha,\phi,0.01)$	SD	%
Feed Rate	A	0.002862	1	0.002862	14.39	6.61	16.3	*	1.26
Spindle Speed	B	0.007310	1	0.007310	36.75	6.61	16.3	**	3.22
Material	C	0.000625	1	0.000625	3.14	6.61	16.3	-	0.28
Grit size	D	0.184900	1	0.184900	929.61	6.61	16.3	**	81.49
Depth of Cut	F	0.010302	1	0.010302	51.80	6.61	16.3	**	4.54
	A×B	0.000400	1	0.000400	2.01	6.61	16.3	-	0.18
	A×D	0.000506	1	0.000506	2.55	6.61	16.3	-	0.22
	B×C	0.009702	1	0.009702	48.78	6.61	16.3	**	4.28
	C×F	0.009506	1	0.009506	47.79	6.61	16.3	**	4.19
	A×B×C	0.000576	1	0.000576	2.90	6.61	16.3	-	0.25
Error	e'	0.000995	5	0.000199	-	-	-	-	0.09
Total	T	0.227685	15	0.226889	-	-	-	-	100.00

Note : S : Sum of Squared Deviation ϕ : Degree of Freedom V : Mean Square F_0 : F-Statistic

SD : Significant Difference (Results of F-Test) * at α = 5.0 %, ** at α = 1.0 %

- **Point Estimate :** $\mu(A_1)+\mu(D_2)+\mu(B_1\times C_2\times F_2)-\frac{T_{III}}{16}\times 2=-0.041875$

- **Interval Estimate :** $\frac{1}{n_e}=\frac{1}{8}+\frac{1}{8}+\left(\frac{1}{4}+\frac{1}{4}-\frac{1}{8}\right)-\frac{1}{16}\times 2=\frac{1}{2}$ $\pm t(\phi_e,0.025)\times\sqrt{\frac{V_e'}{n_e}}=\pm 0.0256$

$$-0.0675<\mu(A_1B_1C_2D_2F_1)<-0.0163$$ (Unit : nm Ra)

Table 2b

Click here to download high resolution image

Factor		S	ϕ	V	F_0	$F(\alpha1,\phi e,0.05)$	$F(\alpha1,\phi e,0.01)$	SD	%
Feed Rate	A	56.2500	1	56.2500	25.40	5.59	12.2	**	44.41
Spindle Speed	B	10.5625	1	10.5625	4.77	5.59	12.2	-	8.34
Material	C	5.0625	1	5.0625	2.29	5.59	12.2	-	4.00
Grit size	D	6.2500	1	6.2500	2.82	5.59	12.2	-	4.93
Depth of Cut	F	12.2500	1	12.2500	5.53	5.59	12.2	-	9.67
	A×B	16.0000	1	16.0000	7.23	5.59	12.2	*	12.63
	C×F	4.0000	1	4.0000	1.81	5.59	12.2	-	3.16
	A×B×D	14.0625	1	14.0625	6.35	5.59	12.2	*	11.10
Error	e'	15.5000	7	2.2143	-	-	-	-	1.75
Total	T	139.9375	15	126.6518	-	-	-	-	100.00

Note : S : Sum of Squared Deviation ϕ : Degree of Freedom V : Mean Square F_0 : F-Statistic

SD : Significant Difference (Results of F-Test) * at α = 5.0 %, ** at α = 1.0 %

- **Point Estimate :** $\mu(A_2 \times B_1 \times D_1) = 0.625$
- **Interval Estimate :** $\frac{1}{n_e} = \frac{1}{4} + \frac{1}{4} - \frac{1}{8} = \frac{3}{8}$ $\pm t(\phi_e, 0.025) \times \sqrt{\frac{V_e}{n_e}} = \pm 2.155$

$$-1.530 < \mu(A_2 B_1 D_1) < -2.780 \quad \text{(Unit : μm)}$$

Table 2c

Click here to download high resolution image

Factor		S	ϕ	V	F_0	$F(\alpha;\phi_1,\phi_e;0.05)$	$F(\alpha;\phi_1,\phi_e;0.01)$	SD	%
Feed Rate	A	6.003	1	6.003	7.33	5.99	13.7	*	0.11
Spindle Speed	B	54.022	1	54.022	65.98	5.99	13.7	**	1.00
Drill size	D	5033.903	1	5033.903	6148.28	5.99	13.7	**	93.53
Vacuum Chuck	G	24.502	1	24.502	29.93	5.99	13.7	**	0.46
	A×C	10.563	1	10.563	12.90	5.99	13.7	*	0.20
	A×D	4.410	1	4.410	5.39	5.99	13.7	-	0.08
	B×C	87.422	1	87.422	106.78	5.99	13.7	**	1.62
	C×F	148.840	1	148.840	12.50	5.99	13.7	*	2.77
	A×B×D	11.903	1	11.903	14.54	5.99	13.7	**	0.22
Error	e'	4.912	6	0.819	-	-	-	-	0.02
Total	T	5386.460	15	5382.386	-	-	-	-	100.00

Note : S : Sum of Squared Deviation ϕ : Degree of Freedom V : Mean Square F_0 : F-Statistic

SD : Significant Difference (Results of F-Test) * at α = 5.0 % ** at α = 1.0 %

- **Point Estimate :** $\mu(G_1)+\mu(A_1\times B_1\times D_2)+\mu(B_1\times C_2\times F_1)-\dfrac{\mu(B_1)}{8}-\dfrac{T_{\cdots}}{16}=29.27$

- **Interval Estimate :** $\dfrac{1}{n_e}=\dfrac{1}{8}+\left(\dfrac{1}{4}+\dfrac{1}{4}-\dfrac{1}{8}\right)+\left(\dfrac{1}{4}+\dfrac{1}{4}-\dfrac{1}{8}\right)-\dfrac{1}{8}-\dfrac{1}{16}=\dfrac{11}{16}$ $\quad \pm t(\phi_e,0.025)\times\sqrt{\dfrac{V_e}{n_e}}=\pm 1.836$

$$27.43<\mu(A_1B_1C_2D_2F_1G_1)<31.10 \quad \text{(Unit : \%)}$$

Table 3a

Click here to download high resolution image

Factor		S	ϕ	V	F_0			SD	%
Spindle Speed	B	0.000915	1	0.000915	49.52	5.99	13.7	**	3.78
Material	C	0.007183	1	0.007183	388.68	5.99	13.7	**	29.70
Grit Size	D	0.001314	1	0.001314	71.11	5.99	13.7	**	5.43
Depth of Cut	F	0.000176	1	0.000176	9.50	5.99	13.7	*	0.73
Vacuum Chuck	G	0.013631	1	0.013631	737.62	5.99	13.7	**	56.37
	A×D	0.000315	1	0.000315	17.05	5.99	13.7	**	1.30
	A×G	0.000203	1	0.000203	10.99	5.99	13.7	**	0.84
	C×F	0.000352	1	0.000352	19.02	5.99	13.7	**	1.45
	A×B×D	0.000077	1	0.000077	4.14	5.99	13.7	-	0.32
Error	e'	0.000111	6	0.000018	-	-	-	-	0.08
Total	T	0.024275	15	0.024183	-	-	-	-	100.00

Note : S : Sum of Squared Deviation ϕ : Degree of Freedom V : Mean Square F_0 : F-Statistic

SD : Significant Difference (Results of F-Test) * at α = 5.0 %, ** at α = 1.0 %

- **Point Estimate :** $\mu(B_2)+\mu(C_1\times F_1)+\mu(A_2\times D_2\times G_1)-\frac{T_{[2]}}{16}\times 2=0.00168$

- **Interval Estimate :** $\frac{1}{n_e}=\frac{1}{8}+\frac{1}{4}+\left(\frac{1}{4}+\frac{1}{4}-\frac{1}{8}\right)-\frac{1}{16}\times 2=\frac{5}{8}$ $\pm t(\phi_e,0.025)\times\sqrt{\frac{V_e}{n_e}}=\pm 0.00821$

$$-0.00653<\mu(A_2B_2C_1D_2F_1G_1)<0.00989$$ (Unit : nm Ra)

Table 3b

Click here to download high resolution image

Factor		S	φ	V	F_0			SD	%
Feed Rate	A	1.5625	1	1.5625	7.69	7.71	21.2	-	3.69
Material	C	5.0625	1	5.0625	24.92	7.71	21.2	**	11.96
Grit Size	D	1.0000	1	1.0000	4.92	7.71	21.2	-	2.36
Depth of Cut	F	1.5625	1	1.5625	7.69	7.71	21.2	-	3.69
Vacuum Chuck	G	20.2500	1	20.2500	99.69	7.71	21.2	**	47.84
	A×D	0.2500	1	0.2500	1.23	7.71	21.2	-	0.59
	A×G	2.2500	1	2.2500	11.08	7.71	21.2	*	5.32
	B×C	4.0000	1	4.0000	19.69	7.71	21.2	*	9.45
	C×F	3.0625	1	3.0625	15.08	7.71	21.2	*	7.24
	A×B×D	1.5625	1	1.5625	7.69	7.71	21.2	-	3.69
	A×B×G	1.5625	1	1.5625	7.69	7.71	21.2	-	3.69
Error	e'	0.8125	4	0.2031	-	-	-	-	0.48
Total	T	42.9375	15	42.3281	-	-	-	-	100.00

Note : S : Sum of Squared Deviation φ : Degree of Freedom V : Mean Square F_0 : F-Statistic

SD : Significant Difference (Results of F-Test) * at α = 5.0 %, ** at α = 1.0 %

- **Point Estimate :** $\mu(A_1 \times G_2) + \mu(B_1 \times C_1 \times F_2) - \frac{T_{[1]}}{16} = 0.6875$

- **Interval Estimate :** $\frac{1}{n_e} = \frac{1}{4} + \left(\frac{1}{4} + \frac{1}{4} - \frac{1}{8}\right) - \frac{1}{16} = \frac{9}{16}$ $\pm t(\phi_e, 0.025) \times \sqrt{\frac{V_e}{n_e}} = \pm 0.9383$

$$-0.2508 < \mu(A_1 B_1 C_1 F_2 G_2) < 1.6258 \quad \text{(Unit : μm)}$$

Table 3c

Click here to download high resolution image

Factor		S	ϕ	V	F_0	[illegible]	[illegible]	SD	%
Feed Rate	A	5.881	1	5.881	6.25	7.71	21.2	-	1.22
Spindle Speed	B	52.201	1	52.201	55.50	7.71	21.2	**	10.85
Material	C	99.501	1	99.501	105.78	7.71	21.2	**	20.67
Drill size	D	189.751	1	189.751	201.73	7.71	21.2	**	39.42
Depth of Cut	F	3.151	1	3.151	3.35	7.71	21.2	-	0.65
Vacuum Chuck	G	70.141	1	70.141	74.57	7.71	21.2	**	14.57
	A×B	20.931	1	20.931	22.25	7.71	21.2	**	4.35
	A×C	14.631	1	14.631	15.55	7.71	21.2	*	3.04
	A×D	7.156	1	7.156	7.61	7.71	21.2	-	1.49
	A×G	13.141	1	13.141	13.97	7.71	21.2	*	2.73
	A×B×D	3.901	1	3.901	4.15	7.71	21.2		0.81
Error	e'	3.762	4	0.941	-	-	-	-	0.20
Total	T	484.144	15	481.322	-	-	-	-	100.00

Note : S : Sum of Squared Deviation ϕ : Degree of Freedom V : Mean Square F_0 : F-Statistic

SD : Significant Difference (Results of F-Test) * at α = 5.0 %, ** at α = 1.0 %

- **Point Estimate :** $\mu(D_2) + \mu(A_1 \times B_1 \times C_1 \times G_1) - \frac{T_{\cdots}}{16} = 27.35$

- **Interval Estimate :** $\frac{1}{n_e} = \frac{1}{8} + \left(\frac{1}{4} + \frac{1}{4} + \frac{1}{4} - \frac{1}{8} \times 2\right) - \frac{1}{16} = \frac{9}{16}$ $\pm t(\phi_e, 0.025) \times \sqrt{\frac{V_e}{n_e}} = \pm 2.02$

$$25.33 < \mu(A_1 B_1 C_1 D_2 G_1) < 29.37 \quad \text{(Unit : \%)}$$

2009-10

Ultra-precision grinding of PZT ceramics--Surface integrity control and tooling design

Arai, S.

Elsevier

Arai S, Wilson SA, Corbett J, Whatmore RW. (2009) Ultra-precision grinding of PZT ceramics - Surface integrity control and tooling design. International Journal of Machine Tools and Manufacture, Volume 49, Issue 12-13, October 2009, pp. 998-1007

http://dx.doi.org/10.1016/j.ijmachtools.2009.05.013